# DEVELOPMENT OF A PLASMON RESONANCE ENHANCED OPTICAL TRAP FOR CHARACTERISATION OF SINGLE METAL NANOPARTICLE

BY

MEHDI ZAMAN

THESIS

Submitted in partial fulfillment of the requirements
for the degree of Master of Science in Mechanical Engineering
in the Graduate College of the
University of Illinois at Urbana-Champaign, 2012

Urbana, Illinois

Adviser:

Assistant Professor Kimani Toussaint, Jr.

## ABSTRACT

The goal of this thesis is to develop an experimental method for constructing a plasmon resonance based gold nanorod trapping platform and suggest methods for characterizing a trapped single nanoparticle. While there are published methods that emphasize on building up an optical trapping setup or trap single gold nanorod using high power lasers, none were found that suggests on constructing a plasmon resonance based optical trapping setup which has the sole purpose of tweezing and characterizing a particular species (aspect ratio) of gold nanorod. Theoretical aspects of plasmon resonance and their contribution in trapping of gold nanorod is studied in detail. Characterisation properties discussed in this thesis include trapping strength, pattern of backscattered light and extinction spectrum. The necessary theories and corresponding equations for trapping force and extinction spectrum estimation are presented including all the assumptions and constraints that were applied. Moreover, the results from these characterisation methods are analysed in order to differentiate between a trapped gold nanorod and a dielectric microsphere. Matlab and LabView codes used in the characterisation experiments are presented at the end of the thesis as attached m-files and vi-files, respectively.

## ACKNOWLEDGEMENTS

This research project would not have been possible without the support of many people. It is difficult to overstate my gratitude to my supervisor, Dr. Kimani Toussaint Jr. for his expert guidance, critical suggestions, kind advice, and constant encouragement throughout the course of my research. I would have been lost without him. I am indebted to all of my colleagues for providing a stimulating and fun environment in which to learn and grow. I am especially grateful to Brian Roxworthy, Raghu Ambekar, and Santosh Tripathi. In particular, I thank Brian Roxworthy for introducing me to optical trapping and guiding me through the fundamental steps. I also thank Tony Lau, Ryan Kovarik and Jie Yee for their friendship and support. Lastly, and most importantly, I wish to thank my parents, Md. Ansaruzzaman, Manjuri Akhter and my sister Maria Zaman. They bore me, raised me, supported me, taught me, and loved me. To them I dedicate this thesis.

# Table of Contents

# Chapter 1

# Introduction

## 1.1 Background and Motivation

Utilizing the momentum of light to immobilize, orient and transport micrometer to nanometer-sized objects within a fluid medium is known as optical trapping. Ashkin[1] pioneered this technique, identifying a number of geometries for using optical forces to levitate and trap dielectric particles [2]. The term optical tweezers [3] refers to a particular geometry where a single laser beam is focused through a high numerical aperture (NA) microscope objective (MO) to generate a three-dimensional trapping volume within a sample medium.

The use of optical forces to trap and manipulate micron-scale particles in solution is a well-acknowledged technique with widespread applications, including the controlled assembly of particles into arbitrary configurations, the precise application of forces to biological structures, from single cells down to single molecules, sensitive particle fractionation, and measurement of many-body colloidal interactions[4]. All these applications would benefit

from the inclusion of optical trapping to nanometer-scale particles. However, the optical gradient force responsible for trapping is proportional to the particle volume in the Rayleigh regime, so that the trapping force on nanoparticles is generally weak and easily overwhelmed by thermal fluctuations (Brownian motion) and by radiation pressure. Only a limited number of experiments have demonstrated stable, three-dimensional tweezing of objects with nanometer-scale dimensions. Objects such as carbon nanotubes [5] and semiconductor nanowires, for example, can be tweezed because of their micron-scale extension in one dimension. As well, gold spheres with diameters down to 20 nm can be trapped by taking advantage of their large refractive index in the infrared [6],but achieving stable, three-dimensional tweezing is difficult [7],and is accompanied by significant heating [8].

By taking advantage of optical resonances, it is possible to overcome many of the aforementioned difficulties by enhancing trapping forces while avoiding very high levels of heating. From experiments conducted in the late seventies, it was observed that Mie resonances enhance the radiation pressure on optically levitated dielectric spheres [9],and the first experimental report of laser tweezers includes a proposal for resonant enhancement of trapping forces[3]. Shortly afterwards, resonant optical trapping of neutral atoms was demonstrated [10], which now serves as the basis of a highly developed technique. Although theoretical work has developed the idea of resonance enhancement for room-temperature trapping of particles in solution[11], experimental success has been limited. Resonances have been shown to slow down the diffusion of single molecules in solution [12], and it has been sug-

gested that excitonic transitions in semiconductor nanocrystals could permit their optical trapping [13], but the trapping forces in these cases are limited by the broad linewidths and low saturation intensities of the transitions. Trapping times at room temperature are therefore limited to a few milliseconds, and stable trapping would require operation at liquid-helium temperatures [14].

Ag and Au nanoparticles, on the other hand, exhibit very strong plasmon resonances that have very high saturation intensities[15]. These resonances are associated with the collective oscillation of conduction electrons in the particle. Using this unique property, various types of metal nanoparticles (particularly those consisting of Au and Ag) such as spherical [16][17], aggregates [18][19], nanorods [20], bipyramids [21], and nanowires [22]have been optically manipulated with a focused laser beam. Additionally, metal nanorods exhibit a strong longitudinal-plasmon resonance, corresponding to electron oscillation along the long axis of the rods, whose frequency can be tuned throughout the visible and nearinfrared frequency range by changing the aspect ratio and composition of the rods [23].

An optical tweezers system can be implemented onto a commercially available research-grade optical microscope[24], which is becoming a popular trend now-a-days. An optical microscope comes with the advantage of having a pre-aligned and robust imaging system that performs traditional methods of high-resolution microscopy (e.g., differential phase contrast,dark field, fluorescence and confocal). Besides, microscopes are also readily available in many biological research laboratories. With well calibrated optical tweezers

built onto an optical microscope system, one can perform precise optical force measurements, while observing them with imaging techniques previously mentioned.

This thesis is targeted at providing a beginner in optical trapping with the basic knowledge necessary to quickly establish an optical tweezers setup that uses plasmon resonance enhanced optical trapping within an inverted optical microscope. Here the presented single-beam optical tweezing setup is built from off-the shelf items, at the same time providing a step-by-step guide to efficiently arrange the optical trains. This thesis also shows how this platform differentiates between a trapped microparticle (dielectric/polystyrene microsphere,radius=1.5 micron) and a gold nanorod (length= 30 nanometer and diameter= 10 nanometer) via stiffness value of the optical trap as well as the backreflected scattering pattern.

For illustrative purposes, we make use of an inverted research-grade optical microscope (IMT2, Olympus). However, all the techniques described herein can be employed on any microscope systems or with opto-mechanical items from other manufacturers to achieve an equivalent performance.

## 1.2 Thesis Organization

In this thesis, the unique phenomenon of tweezing a gold nanorod using plasmon resonance enhancement and later its characterization is explored. Starting from the very first chapter, the background, motivation and appli-

cations of optical trapping are explained. In chapter two, the theoretical groundwork for optical tweezing is presented detailing on the two fundamental regimes that dominate the tweezing mechanisms. In the following chapter, the idea of optical tweezing is materialized by delineating the construction mechanism of a full working optical tweezing setup using an inverted optical microscope as a robust platform. Full equipment setup and procedure are provided along with the experimental design. In the fourth chapter, plasmon resonance enhancement in successful tweezing of single and double Au nanorod is investigated with suitable theory and application. Chapter five describes a spectroscopic characterisation procedure for the trapped Au nanorod. Experimental methods as well as results are presented and discussed with observed pitfalls and necessary suggestions. The last chapter i.e. chapter six elucidates upon a side-by-side comparison between polystyrene microsphere and Au nanorod tweezing in terms of instrumentation requirement as well as characterizing them using different metrics. In addition, it elaborates upon the theoretical aspect of measurement of trapping stiffness and is concluded with using the corner frequency and their corresponding stiffness values as characterisation metrics to differentiate between the trapping of two different particles. Subsequently, another method of characterization is analyzed where the investigated feature is the backscattered light (which infact is the trapping wavelength of 785nm) from the trapped gold nanorod. Difference between the collected pattern and integrated intensity values are examined as means of characterization metrics between the trapped particles.

# Chapter 2

# Optical Tweezers: Theory

## 2.1 Introduction

Optical trapping occurs due to radiation pressure originating from the scattering, emission, absorption or retardation of photons. The dominant type of radiation pressure in optical force traps is known as the gradient force, which is the force on a trapped object due to gradient of trapping beam. The gradient force is proportional to the spatial gradient in light intensity and acts in the direction of the gradient [3]. Although the terms 'trapping' and 'tweezing' are used interchangeably, 'optical trapping' mainly refers to the restriction of the movement of the particle of interest against Brownian motion, whereas 'optical tweezing' refers to the manipulation of the position of the particle in a three-dimensional volume. The experimentations in this thesis deal mostly with 'optical tweezing' rather than 'optical trapping'.

For laser tweezers, the reason for the variation of gradient force depends

on the scale of the wavelength of light used compared to the scale of the object being trapped. In the Rayleigh regime, the diameter of the object is much smaller than the wavelength of light and light traveling through the object induces a dipole on the object. The object then can be thought of as a dipole in an electric field. The result of this is that the object feels a time-averaged force in the direction of the light gradient, which is known as the gradient force[25].

In the Mie regime, where the wavelength of light is much smaller than the diameter of the object, ray-optics can be used to explain the gradient force. Given a spherical object whose index of refraction is larger than the surrounding medium, light will be bent in such a way that the momentum change of the light will be in the opposite direction of the light gradient. Following Newton's third law, the object will gain momentum in the opposite direction, i. e., in the direction of the light gradient[26].

By focusing a monochromatic beam through a convex lens, creation of a light gradient is possible which is able to trap at the focus of the lens. Trapping occurs when the gradient force is the dominant force. Other forces of significance are the scattering force and Langevin force. The scattering force is caused by the change of momentum of reflected light. However, its overall effect can be further reduced by using a microscope objective with high numerical aperture. The Langevin force is the random force occuring from Brownian motion. For most applications, especially in the biological field, Brownian motion cannot be significantly reduced due to temperature restrictions and therefore is the dominant effect that determines the minimum

power required to create an effective laser trap [27].

## 2.2 Ray Optics and the Mie Regime

In the Mie Regime, where an object to be trapped is much larger than the wavelength of light used, ray optics can be used to explain trapping since it plays the dominant role in trapping the object. Given a transparent sphere

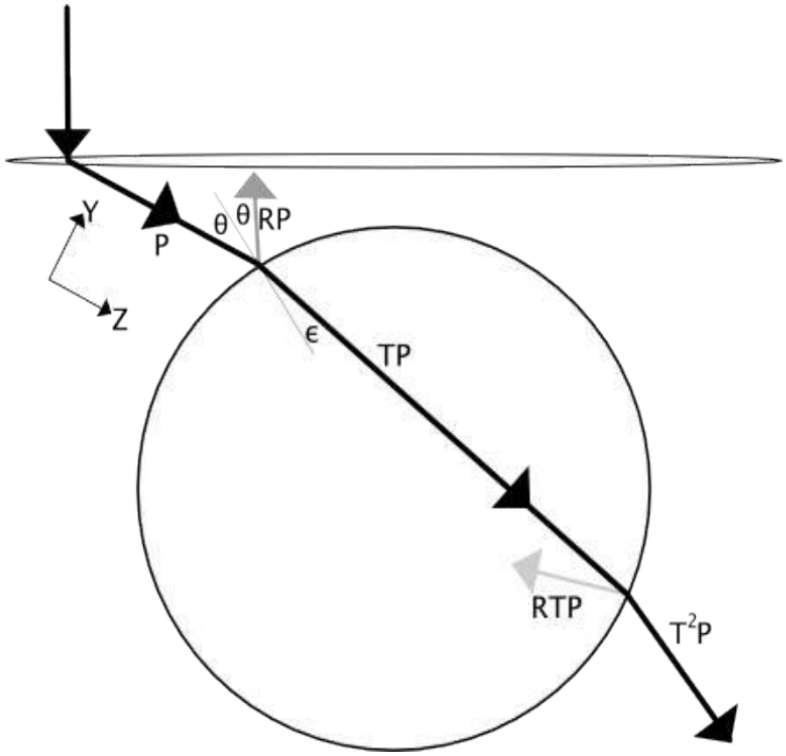


Figure 2.1: A single ray passing through a transparent bead (Ray optics diagram). The diagram depicts one ray of light being bent by a microscope objective and passing though a transparent bead. P is the incident power, RP is the first reflection, TP is the light transmitted into the bead, RTP is the reflection from the internal wall of the bead , $T^2P$ is the light that finally exits the bead. Here, $\theta$ and $\epsilon$ are the angles of reflection and refraction [27].

in a medium where the size of the sphere is much greater than the wavelength of light and given a known distribution of parallel rays focused to a point with a microscope objective (diffraction can be ignored for Mie regime) and given that the sphere is close enough to the focus of those rays, the force, $F$, due to a single ray of power $P$, is given by [26]

$$F_Z = \frac{n_m P}{c}\left[1 + R\cos 2\theta - \frac{T^2[\sin(2\theta - 2\epsilon) + R\cos 2\theta]}{1 + R^2 + 2R\cos 2\epsilon}\right], \tag{2.1}$$

and

$$F_Y = \frac{n_m P}{c}\left[R\sin 2\theta - \frac{T^2[\sin(2\theta - 2\epsilon) + R\sin 2\theta]}{1 + R^2 + 2R\cos 2\epsilon}\right] \tag{2.2}$$

where $\theta$ is the angle of incidence, $\epsilon$ is the angle of refraction, the $Y$ and $Z$ components are perpendicular and parallel to the the direction of the incident ray respectively, and $R$ and $T$ are the Fresnel reflection and refraction coefficients (Figure 2.1)[25]. $F_Z$ is the scattering force and $F_Y$ is the gradient force as in Ashkin's work[26]. The total net force is the vector sum of all the forces of every ray traveling through the bead.

The trapping forces in the Mie regime do not depend on sphere size. Also the trapping forces increase with $\theta$ ,which means that the rays along the outer edge of the laser contribute more to the trapping force than the rays going through the center, which also means that using a high numerical aperture objective will trap a bead with more force. Therefore, in building an optical trap, the laser should slightly overfill the back aperture of the microscope objective and a lens of the highest possible numerical aperture should be used [26]. However, under certain circumstances, with very steep

gradients, ray optics predicts that a higher numerical aperture can decrease trapping efficiency. This contradicts theory in the Rayleigh regime and this is where the theories for the two regimes differ.

## 2.3 Electromagnetic Theory and the Rayleigh Regime

The Rayleigh regime is where the object to be trapped is much smaller than the wavelength of light. In this limit, the object can be thought of as a point induced dipole in an electromagnetic field. Again the two components of the total force associated with optical tweezing are the dissipative scattering force acting in the direction of light propagation and the conservative gradient force acting in the direction of the gradient of light intensity due to the focused beam. For stable trapping, the gradient force must exceed the scattering force in order to create a potential well deeper than the thermal energy of the particle originating from Brownian motion. When the particle is much smaller than the wavelength, the instantaneous field can be approximated as uniform, and the particle is treated as an induced dipole oscillating in a time-harmonic field. The induced dipole adheres to the following rule [28]:

$$\vec{p} = \varepsilon \alpha \vec{E}, \tag{2.3}$$

where $p$ is the dipole moment, $\varepsilon$ is the vacuum electric permittivity, and $E$ is the applied electric field. The complex polarizability, $\alpha = \alpha' + i\alpha''$, arises from the lag in phase between the applied electric field and the induced dipole. The optical forces applied to the dipole are determined using the

Lorentz force. These time-averaged forces are [28]

$$\langle \vec{F}_g \rangle = \frac{\varepsilon}{4} \left[ \widehat{x_j} \frac{d}{dx_j} ({E_k}^* \alpha') E_k \right] \tag{2.4}$$

and

$$\langle \vec{F}_s \rangle = \frac{\varepsilon}{2} Im \left[ \widehat{x_j} E_k^* \alpha'' \frac{dE_k}{dx_j} \right] \tag{2.5}$$

where $\widehat{x_j}$ are the Cartesian unit vectors, $E_k$ are the components of the electric field magnitude, $F_g$ is the gradient force, and $F_s$ is the scattering force. To predict these forces, the polarizability and electric field must be known. The spatial distribution of the electric field is described with a paraxial (zeroth-order) Gaussian beam focused by a lens [29]. The scattering and gradient forces that result from this electric field scale with the real and imaginary parts of the complex electric polarizability, respectively. So the maximum of the real and imaginary parts of the electric polarizability will also represent the maximum of the gradient and scattering forces, respectively.

# Chapter 3

# Optical Tweezers: Construction

## 3.1 Experimental Design

Continuous wave lasers form the fundamental instrument for optical tweezing. The key properties that are examined for choosing a good tweezing laser include the $M^2$ factor of the laser, its maximum optical power, pointing stability, power amplitude fluctuations, and laser wavelength. In order to generate a high-quality three-dimensional optical trap a high numerical aperture (NA) microscope objective (typically 1.4) is often used. With high-NA objectives, the lateral and axial gradient forces in the optical tweezers are optimized to trap an object in three dimensions. Infinity-corrected objectives are the most commonly used, as they offer the highest flexibility in trapping systems [2].

By overfilling the back aperture of a high NA oil or water immersion objective with a Gaussian beam ($M^2 < 1.1$) a good-quality optical tweezers are produced which in turn also produces a diffracted-limited trapping spot. Essentially, when a well-collimated Gaussian beam overfills the back aperture of the high NA objective (about 10%) , it is possible to obtain a single-beam optical trap. Additionally, a beam-steering mirror system may be constructed to ensure that the single-beam optical trap can be steered across the sample without the collimated beam walking off its position at the back aperture of the objective. The beam-steering mirror system relays the image of the steering mirror onto the back aperture of the objective. As a result, any tilt (angular adjustment) in the steering mirror will result in a direct lateral translation of the optical tweezers beam spot at the sample plane [2].

The position of the trapped particle may be estimated by imaging its interference pattern at the back focal plane of the collecting objective onto a quadrant photodiode (QPD). A semiconductor material, silicon (Si) or indiumgalliumarsenide (InGaAs) forms the QPD and each material operates over a characteristic wavelength range, that is, 250-1100 nm for silicon and 1000-2000 nm for InGaAs. For tracking optically trapped particles, the forward or backward-scattered light signals from the tweezing beam (or an auxiliary probe beam) can be collected or imaged onto the QPD. The response of the detector to the appropriate wavelength is critical to both a faster time response and greater position sensitivity [2].

The first part of the following protocol makes use of the schematic diagrams

(Figs. 3.1 and 3.2) as guides for planning the optical arrangements for the tweezers setup. In our setup, the optical train is made up of two parts: a beam expansion telescope that matches the beam size to the back aperture of the objective (red-dotted box in Fig. 3.1) and a beam-steering mirror system (blue-dotted box in Fig. 3.1) that steers the trapping beam onto the back aperture of the trapping objective. The second part of the protocol describes the steps to optimize the optical alignment so as to achieve a diffraction-limited spot.

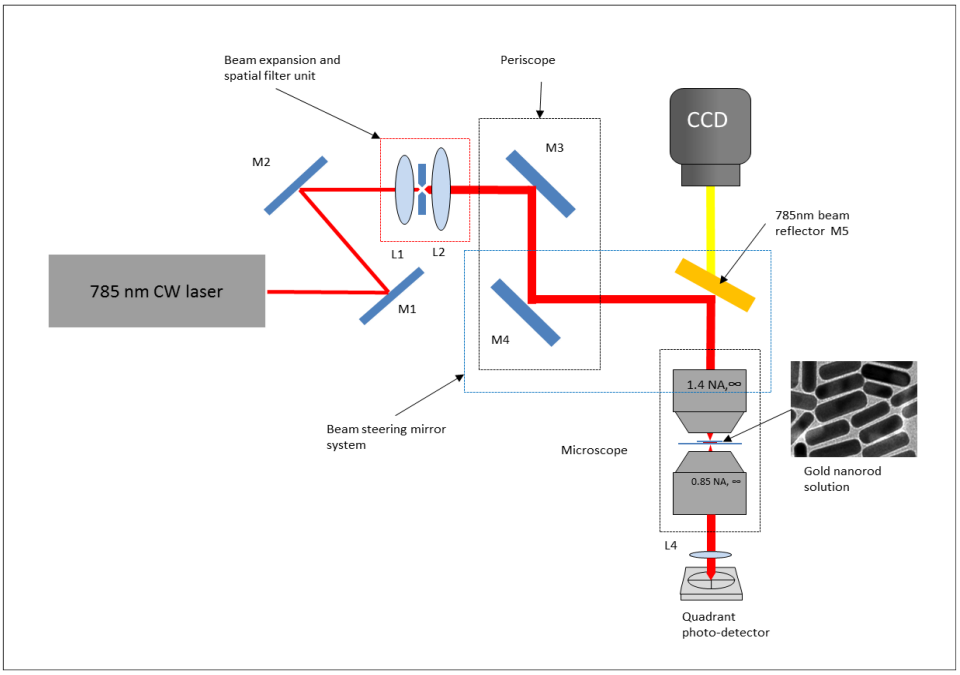


Figure 3.1: Schematic of the experimental setup.

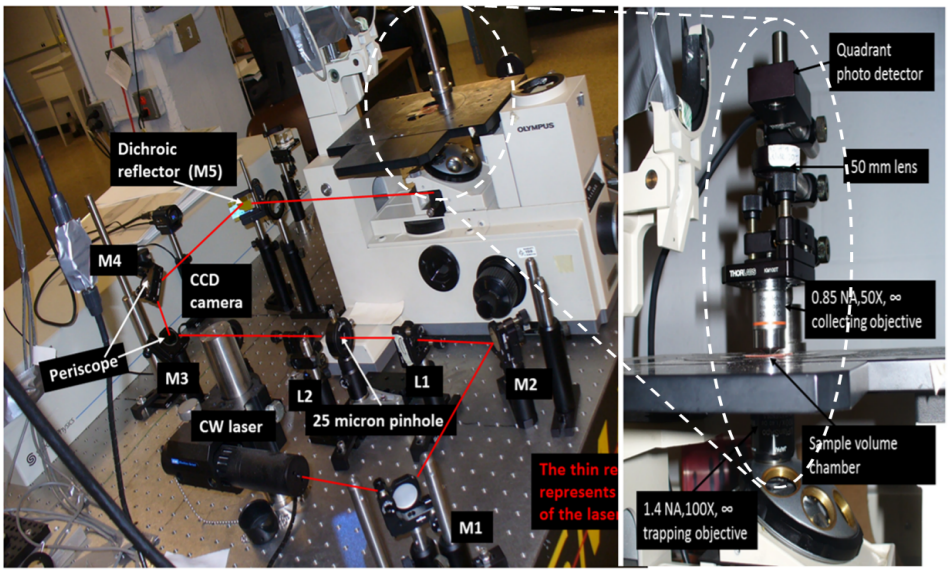


Figure 3.2: Photograph of the actual experimental setup. A collimated laser beam from a 785 nm diode laser ($M^2 < 1.1$, maximum optical power of 130 mW) is used for trapping (solid red line). The beam path used for trapping consists of lenses L1(50mm) and L2 (150mm) for 3:1 expansion of beam (beam diameter increases from 3mm to 9mm) and for spatial filtering the beam was let pass through a 50 micron pinhole between the lenses. This expansion of the beam enables slightly overfilling of the back aperture of the trapping objective (trapping objective back aperture diameter is about 7mm).M1 and M2 are broadband silver coated mirrors used for redirecting the beam towards the periscope. The periscope consisting of mirrors M3 and M4 is used for elevating the beam to the microscope back aperture height. A 785 nm beam reflector/dichroic mirror(DM) (FF746 sDi01-25X36X3.0mm,Semrock Inc.) was used to redirect the trapping beam (which also lets pass the visible wavelength towards the CCD camera at the same time) towards the back aperture of the trapping objective through the epifluorescence port of the microscope. Mirrors M4 and the DM (M5) form the beam steering system. The 1.4 NA,infinity corrected, 100X oil immersion objective was used to focus the 785 nm beam into the gold nanorod solution. Lens L4 was used to image the back focal plane from the collecting objective (0.85NA,50X,infinity corrected) onto the quadrant photo-detector (THORLABS, PDQ80A).The back scattered light from the trapped nanorod was imaged onto a CCD camera (WATEC 902H). The focal lengths of the lenses are as follows: L1=50mm,L2=150mm and L4=50mm.

## 3.2 Equipment Setup

The construction of a single-beam optical trap onto an inverted optical microscope is straightforward and requires very little custom fabrication. Most components are mounted with optical supports that are firmly screwed into a vibration damped (floated) optical table. In the presented design only a single laser source and a single QPD is used [2]. The diode laser source has an excellent beam quality ($M^2 < 1.1$), which is essential for achieving a diffraction-limited trapping volume. The polarization of the beam was kept linear. The power of the trap beam was kept constant at approximately 65 mW at the input to the trapping objective. Several broadband silver coated mirrors were used to steer the beam onto the epifluorescence port. The usage of multiple mirrors provided an easy mechanism for accomodating a long optical path on a small bench and obtaining necessary optical conjugates for beam steering and at the same time for avoiding beam walk off. These initial optical alignments are substantial in obtaining a diffraction-limited spot or Airy disk, which is in turn fundamental to the production of a high-quality three-dimensional single-beam optical trap. The microscope body may be placed near the edge of a floated optical table to allow adequate space to accomodate the optical train. The optical tweezing beam was delivered to the trapping objective through the epifluorescence port of the microscope. The user may choose to place the optical elements within a black acrylic case with a lid for the purpose of exclusion of room lights, interfering air currents and reducing the amount of dust settling on the optics [2]. The overall layout of the optical system is illustrated in the schematic shown in

Figure 3.1. Figure 3.2 shows a photograph of the actual setup with labels.

## 3.3 Procedure for setting up the experiment

### 3.3.1 Arrangement of the optical train for the single-beam optical trap

1. The height of the laser was set such that it was 10-15 cm above the top of the optical bench and aligned along one of the rows of the threaded holes of the optical table.

2. Using two silver coated mirrors the collimated laser beam was redirected towards the periscope. In order ro realign the beam two irises were used in conjunction with two mirrors (Thorlabs,PF10-03-01).

3. Using the values of the diameter of the back aperture of the trapping objective and the beam waist of the laser, the focal lengths required for a simple two-lens beam expander combination were calculated (lenses L1 and L2). This 4f arrangement was used to expand the beam so as to overfill the back aperture of the objective by around 10%. The lenses L1 and L2 were used to form a 3:1 beam expander that expanded the collimated laser beam from a diameter of 3 to 9 mm in order to slightly overfill the back aperture of the objective (diameter 7mm).

4. The separation of the lenses were finely adjusted to achieve a collimated beam at the output of the beam expander; the collimation was tested over at least 1-2m.

5. The second part of the optical train was constructed at a height that coincides with the entry point of the expanded laser beam into the microscope. At this point, It was easiest to arrange the optics at the new height and then link the two beam paths using the periscope (M3 and M4) and a redirecting dichroic mirror (M5). The dichroic mirror DM(M5) was placed at an appropriate distance from the epi-fluorescence port of the microscope such that the redirected beam from the DM is incident upon the mirror just below the trapping objective. The height from the bench-top to the centre of this mirror was measured, which defined the height at which the beam steering system was positioned. The DM was chosen to be a 785 nm beam reflecting mirror from Semrock Inc.(FF746 sDi01-25X36X3.0mm), which fits snugly into the right-handed adjustible height kinematic rectangular optic mount (KM100C, Thorlabs Inc.) which was used in conjuction with the upper part of the periscope to change the lateral position of the beam entering the back aperture of the trapping objective.

6. The microscope body was aligned parallel to the rows of threaded holes of the optical bench. The beam redirected from the DM was brought into the trapping objective via the silver coated mirror just beneath the objective. The collimation of the beam was checked with two irises positioned between the microscope back aperture and the dichroic mirror.

7. In order to check that the beam was centered at the back aperture of the trapping objective, the DM was tilted over a suitable range of

angles. A marked pointer was placed onto a piece of transparent tape that was stuck over an objective mount and an infrared (IR) viewer was used to view the beam. Before steering the mirror M5, it was checked that the beam is aligned with the principal axis of the condenser.

### 3.3.2 Alignment of a diffraction-limited spot for the single-beam optical trap

1. A CCD camera (Watec,902H)was placed behind the DM in order to view the trapping phenomenon and collect the back scattered light from the trapped nanoparticle.

2. A clear microscope glass slide was placed on the sample holder of the microscope stage and microscope focusing knob was adjusted until Airy disks were observed from the (4%) back-reflected light of the microscope glassair interface. The fine focus was adjusted until the size of the Airy disks was minimized. When the image of the trapping beam was first observed at the focus of the microscope, there was a high probability that aberrations will be present because of slight misalignment in the optical train. Assuming that the above procedure is followed and the beam remains relatively close to the principal axis of the optical train, many aberrations were corrected using a simple iterative procedure (Steps 10 and 11).

3. The steering mirror M5 was adjusted in order to place the observed Airy disks to the center of the field of view.

4. The mirror M4 was adjusted in tandem with M5 until the Airy disks

appeared symmetric. The fine focus of the microscope was varied to observe the symmetry of the Airy disks as they expand and contract. Any other beam asymmetry was detected and adjusted accordingly.

5. Step 4 was repeated until the beam was centered in the field of view and exhibited a circularly symmetric Airy disk pattern that expanded and contracted when the fine focus of the microscope was adjusted.

# Chapter 4

# Optical Tweezing Using Surface Plasmon Resonance

## 4.1 Introduction

For centuries, scientists have been intrigued by the interaction of light with matter. Metal nanoparticles exhibit intense colors (e.g., ruby red for gold nanoparticles, and yellow for silver) which has inspired not only many scientists but many artists also. Metal nanoparticles are used as colorants in glasses due to dispersion of intense colors, and as a result have been used to decorate windows of many cathedrals, palaces, etc. Since Michael Faraday showed a simple way to synthesize stable dispersions of metal nanoparticles (gold) by a chemical route in 1857 [30], scientific enquiry started quite heavily on this topic [31]. Faraday showed that metal nanoparticles having sub-wavelength dimensions exhibit intense colors, which are quite different than the original bulk metal. The colors of dispersions of metal nanopar-

ticles was explained by Gustav Mie in 1908 using classical electromagnetic theory [32].

The source of the observed intense color can be attributed to strong absorption and scattering of light by dispersion of metal nanoparticles. A strong absorption band is usually seen in the visible region of electromagnetic spectrum of noble-metal particles, which arises from a resonance between collective oscillations of conduction electrons with incident electromagnetic radiation. Since incoming field induces polarization of conduction electrons compared to the heavier ions, electric dipoles form. A restoring force is created by the net charge difference between the electrons and the ions. The resonance between frequency of oscillation of electrons and frequency of incident photons is known as plasmon resonance, which is characterized by a strong absorption band. Since at the surface of a nanoparticle the net charge difference is felt, the resonance is known as surface plasmon resonance (SPR) [31].

Gold and silver nanoparticles have been studied much more extensively compared to other metallic nanoparticles because of their unique optical properties. Gold and silver nanostructures exhibit tunable optical properties over wide spectral ranges and their SPR band usually lie in the visible range of electromagnetic spectrum. Various factors such as size and shape as well as the relative permittivity of the medium determines the SPR bandwidth and the peak maximum [33].

The SPR band is widely tunable from the visible to the near-infrared ranges by varying the shape of the nanoparticles [34], whereas the changing the size

has negligible effects on the SPR band. Changing the shape from spherical to rod-like, two plasmon bands is generated from a single broad plasmon absorption band. The transverse plasmon resonance creates the peak at the shorter wavelength, whereas the longitudinal plasmon resonance creates the peak at the longer wavelength. By changing the aspect ratio [35] the longitudinal plasmon band is tunable from visible to near-infrared, whereas the transverse plasmon band is insensitive to nanoparticle morphology.

## 4.2 Theory

The gradient restoring force by overcoming the scattering force ensures stable trapping of a nanoparticle. For trapped nanoparticles whose absorption spectrum consists of a resonance peak, the trap strength will depend on the shape and location of the absorption peak [21][28]. It is assumed that no

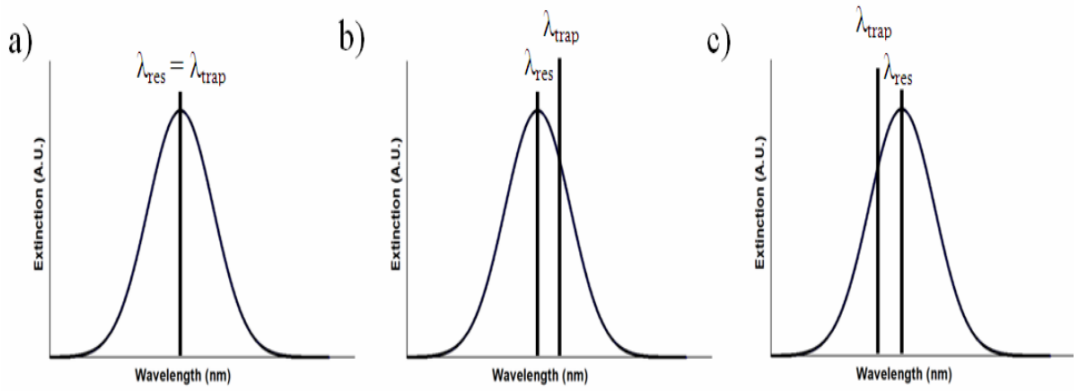


Figure 4.1: Three regimes of resonance absorption and trapping wavelength are shown [28].

trapping takes place when the trapping beam wavelength is equal to the absorption curve peak wavelength, where the scattering force is maximal and gradient force is zero (Figure 4.1(a)). Trapping strength increases as the beam wavelength is red detuned from the resonance absorption peak of the trapped nanoparticle. Trapping strength diminishes as the trapping wavelength is increased/further red detuned. (Figure 4.1(b)). If the trapping wavelength is blue-detuned from the resonance wavelength, trapping strength again diminishes since the gradient force diminishes away from the most intense region of the beam/resonance peak [28] (Figure 4.1(c)).

Figure 4.2 and 4.3 shows the simulated [36] scattering and absorption cross-

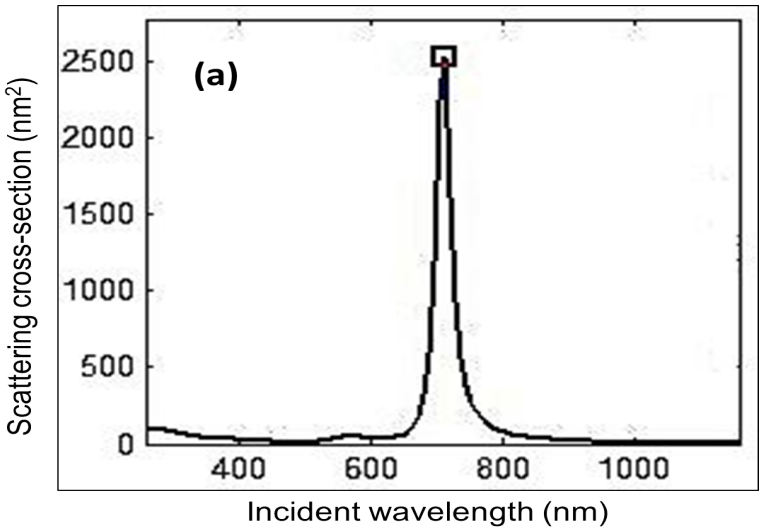


Figure 4.2: Simulated scattering cross-section for the longitudinal plasmon mode of a single Au nanorod in water with length 30 nm and radius 10 nm.

sections for the longitudinal plasmon mode of a Au nanorod with length 30 nm and radius 10 nm, and surrounding medium $\varepsilon_m$ =1.77(water). The

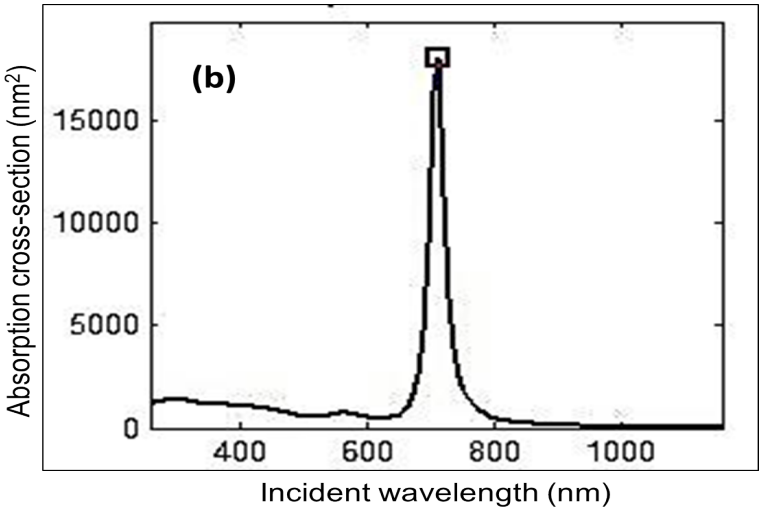


Figure 4.3: Simulated absorption cross-section for the longitudinal plasmon mode of a single Au nanorod in water with length 30 nm and radius 10 nm.

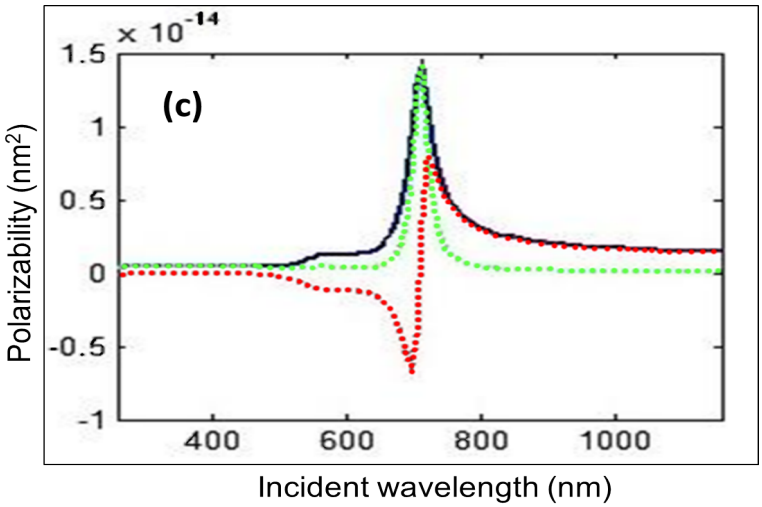


Figure 4.4: Real part (red curve) and imaginary part (green curve) of electric polarizability for an prolate spheroid (mathematical approximation of Au nanorod) with principal axis parallel to the direction of polarization of the optical field.

resulting plasmon occurs at 710 nm wavelength, and the cross-section for absorption is multiple times that of scattering. The real and imaginary part of polarizability acting on the Au nanorod is shown in Fig. 4.4. The real part of the polarizability reaches a maximum at about 725 nm, which is the same wavelength at which the gradient force reaches a maximum. The gradient force or, the real part of the polarizability is significantly increased when the trap laser wavelength is detuned to the long wavelength side of the longitudinal plasmon resonance. Hence, for the current experiment a trapping laser wavelength of 785 nm is chosen, at which wavelength the gradient force(or, real part of polarizability) is significantly higher than the scattering force (or, imaginary part of polarizability).

## 4.3 Gold Nanorod Solution Preparation

Gold nanorod solution in the form of a colloid solution was bought from NANOPARTZ Inc. (Loveland CO.) in a bottle containg 25 mL of solution. The nanorods were contained in DI water with 0.1% ascorbic acid and 0.1% CTAB surfactant capping agent. CTAB is used in manufacturing and its concentration is important in keeping the product from aggregating. Solutions were created such that the sample to be used with the optical trapping setup contains 1-2% of original solution from the bottle. In order to do so first about 10 microlitres of original gold nanorod solution was taken into a pipet tube where additional amount of DI water was poured in order to fill up the entire pipet tube(about 400 microlitres).Using DI instead of normal

water can help reduce heating effects from an infrared (IR) laser. Then from this intermediate solution about 80 microlitres were taken into the volume chamber created by putting a rubber gasket (0.12mm deep) on a 24mm by 60 mm cover glass, which was later placed in the sample plane of the microscope.

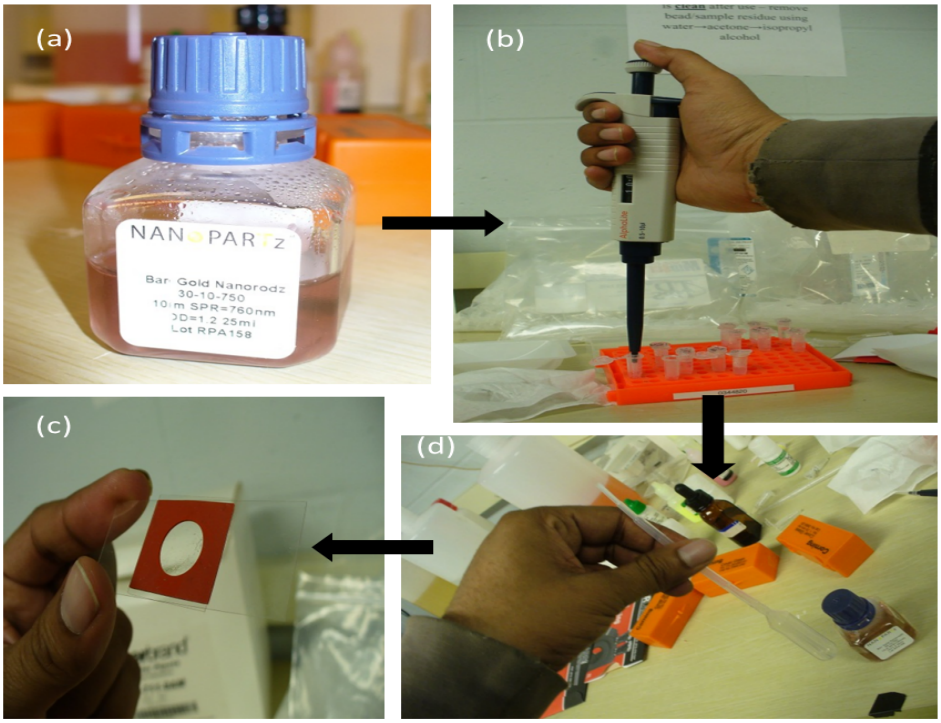


Figure 4.5: Gold nanorod solution preparation procedure.(a) Gold nanorod solution bottle (b) Using Alphalite pipettors to extract about 10 microlitres of solution from the orginal bottle and inserting into a micro pipette (c) Taking the solution from the micro pipette into the transfer tube and mixing the solution by manual circular agitation (d) Using the mixed solution onto the cover glass in order to create the sample.

## 4.4 Experimental Setup

The experimental setup used for this experiment is the same described in the previous chapter.

## 4.5 Results and Discussion

### 4.5.1 Trapping Trajectories

Representative time traces, termed trapping trajectories, of gold nanorods are shown in figure 4.6. All the particle types studied here were aligned in the optical trap due to their anisotropy in shape and optical resonance. The CCD detector was used to record time trajectories created by the backscattered light from the trapped particle. This recording was conducted over the duration of 4-5 hours. During the first hour no nanorods entered the trap and only detector white noise was recorded. Shortly after 1 hour a nanorod entered and remained in the trap. The spikes in the trajectories were typically observed when a particle entered the trap.

A single particle entered the trap at 60 min followed by a second particle at 100 min. The fact that the signal intensity is simply doubled by the addition of the second particle is probably because the latter nanorod is identical to the first. Due to limited trap laser power and lower particle concentration only two particles were seen trapped. Assuming that a single step or plateau in the time trajectory was equivalent to 1 particle in the trap, from the figure we can see a uniquely informative trajectory of sequential loading

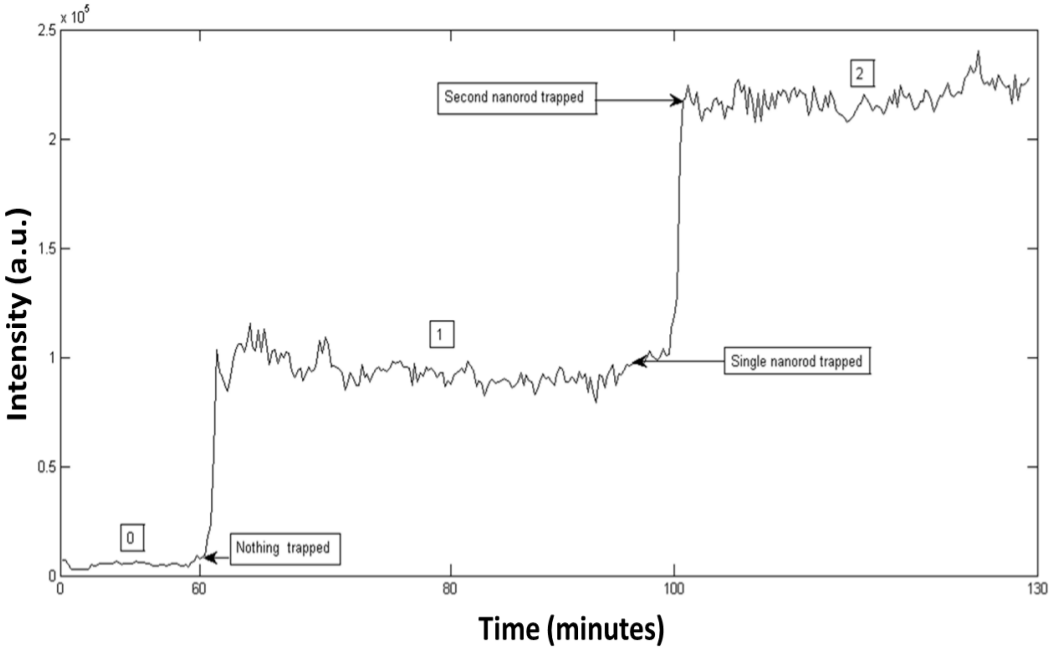


Figure 4.6: Time trace showing loading of Au nanorods integrating over 752(horizontal)x582(vertical) pixels of the CCD. The numbers 0-2 label the stepwise signal level changes that occur as particles are progressively loaded into the trap.

of Au nanorods. Two distinct steps or plateaus (labeled 1-2) were observed relative to the baseline (labeled 0), of sequential particle addition.

# Chapter 5

# Measurement of Extinction Spectrum of a Trapped Gold Nanorod

## 5.1 Introduction

In this chapter, we demonstrated a straightforward method for simultaneous optical trapping and spectroscopy of individual nanoparticles in solution using a single-beam optical tweezer, combined with dark-field microscopy. The objective of this experiment was to study the influence of plasmonic coupling on optical trapping by combining 3D optical trapping with darkfield Rayleigh scattering spectroscopy, enabling us to investigate the interaction of metal nanoparticles inside an optical trap and its evolution in time.

## 5.2 Experimental Setup

The optical tweezers were built on an inverted microscope (Olympus IMT2) using a near-infrared (NIR) diode laser operated at 785 nm. To measure elastic scattering spectra from trapped single particles, we used a dark-field microscope configuration similar to that used in experiments Mock et al. [37]. Figure 5.1 schematically illustrates the setup. The experimental

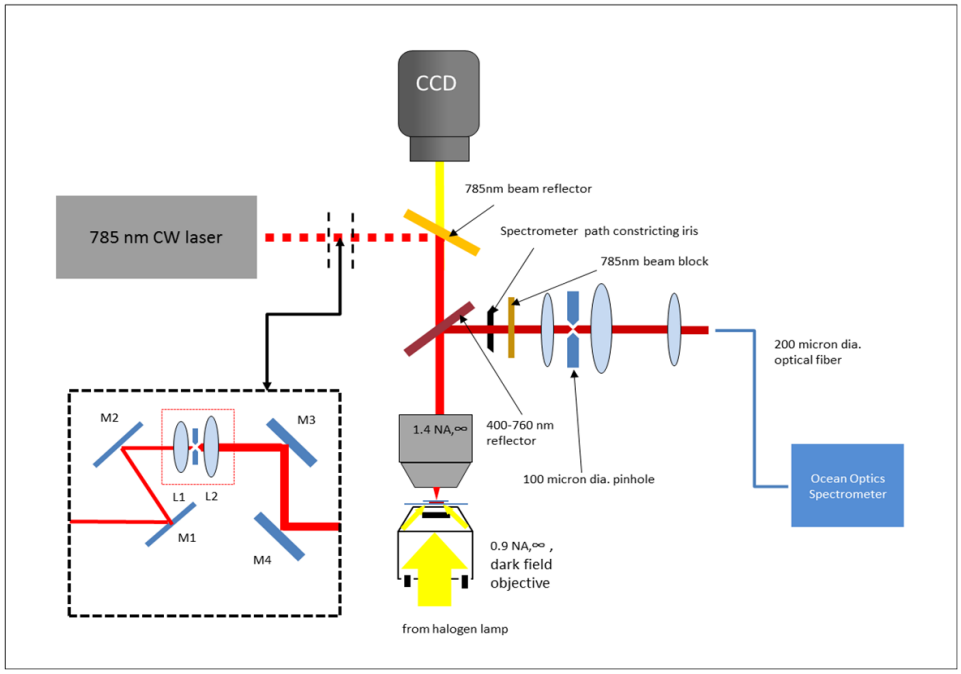


Figure 5.1: Sketch of the experimental setup used for simultaneous 3D optical trapping and Darkfield Rayleigh scattering microscopy.

arrangement introduced in this chapter is suitable for darkfield Rayleigh scattering spectroscopy on optically trapped nanoparticles. Since optical trapping relies on a gradient of the optical field density, a tight focusing of the trapping laser beam is required. This is provided by objective lenses with

high numerical apertures (NA). Typically, metal nanoparticles are trapped in 3D using 1.4 NA objectives.

Laser tweezer operating at 785 nm were coupled into an Olympus IMT2 inverted microscope equipped with a diode laser (Power Technology Inc., IQ2C), as shown schematically in Figure 5.1. The NIR laser beam was focused by a 100X oil-immersion objective (Olympus 1.4 NA,infinity corrected) to a diffraction limited spot into the sample, where the power used ranged between 60 and 65 mW. The laser polarization was kept linear. The forward scattered white light was collected by the trapping objective.

In contrast to optical trapping, darkfield microscopy was performed to ensure that only scattered, but not straight, light was collected by the objective lens. The limitation was imposed by the existing darkfield condenser (Olympus dry 0.90 NA,100X). This mutual incompatibility aspect of the two techniques straitened their integration so far. To resolve this issue, the NA of the objective lens was constricted only in the spectroscopy channel, keeping the numerical aperture intact for the trapping laser path. Due to the fact that most of the modern objectives are infinity corrected, the NA of such objectives can be varied by an iris installed anywhere between the objective back aperture and the tube lens. It is believed that the ease of implementing this solution will promote the optical trapping with darkfield microscopy to become a standard tool for simultaneous 3D optical manipulation and imaging/spectroscopy of metal nanostructures.

A halogen lamp was used to illuminate the sample at large angles from above through a dark-field condenser. A dichroic mirror (Semrock, FF757-

Di01 25X36) transmitted the infrared trapping beam and reflected the elastically scattered light between 400 and 760 nm to reach the spectrometer. In between this dichroic reflector and the spectrometer a 785nm beam block (SP01-785RS-25) was used which obstructed the leaking 785 nm from the dichroic to be incident on the spectrometer. Just before the spectrometer a pinhole was used to spatially select the scattered light. The scattering spectra were collected by a spectrometer (Ocean Optics, spectral resolution 1 nm), which was connected to the microscope using an optical fiber (Ocean optics, 200 micron diameter). Scattering spectra were corrected for spectral variations in system response as well as for white-light intensity distribution through division by bright-field spectra recorded through the sample cell.

## 5.3 Results and Discussion

Both darkfield Rayleigh scattering spectroscopy and imaging of single Au nanorod sequentially diffusing into the trap were systematically performed. Images have been recorded with a digital camera (Watec 902H) at 29.96 frames per second. Scattering spectra have been acquired using a spectrometer (Ocean optics USB2000). Due to the construction of our microscope, both imaging and spectroscopy were simultaneously performed in the same experiment.

The objective of this experiment is to acquire extinction (summation of absorption and scattering) spectrum of a single gold nanorod fixed in the

optical trap. In order to do so, first we used a Matlab simulation [36] in order to find out the scattering spectrum of a single gold nanorod. According to the code the spectrum has a peak at 710 nm of incident white light. The simulated extinction spectrum is given below (Figure 5.2). The

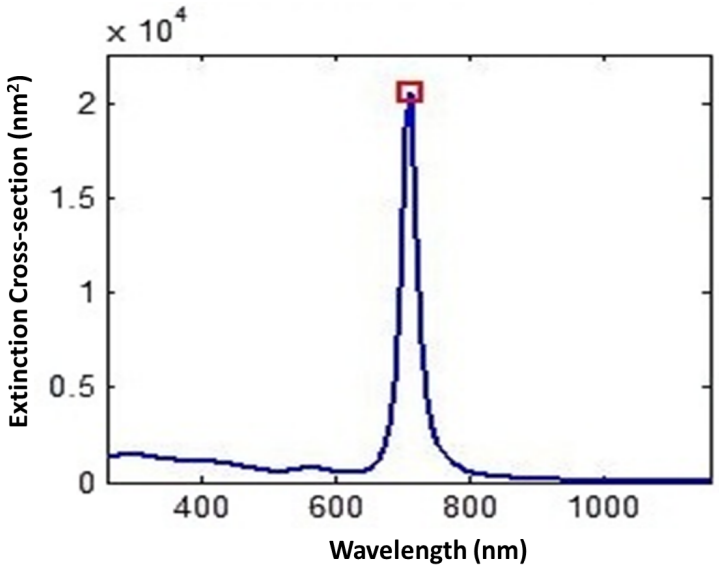


Figure 5.2: Simulated extinction spectrum of a single gold trapped nanorod.

peak of this spectrum is blue shifted fromn the peak (750nm) of the spectrum of the original solution (Figure 5.3). This difference in the location of the peak position for a single trapped nanoparticle from the ensemble was also evident in [38]. Which also suggests that from our experiment, the extinction peak of the single trapped gold nanorod should be around 710 nm.

The spectrum obtained from our experiment for a single trapped gold nanorod is shown in Fugure 5.4. However, from figure 5.4, a peak can be seen somewhere around 778nm. Which could be the consequence of a number of

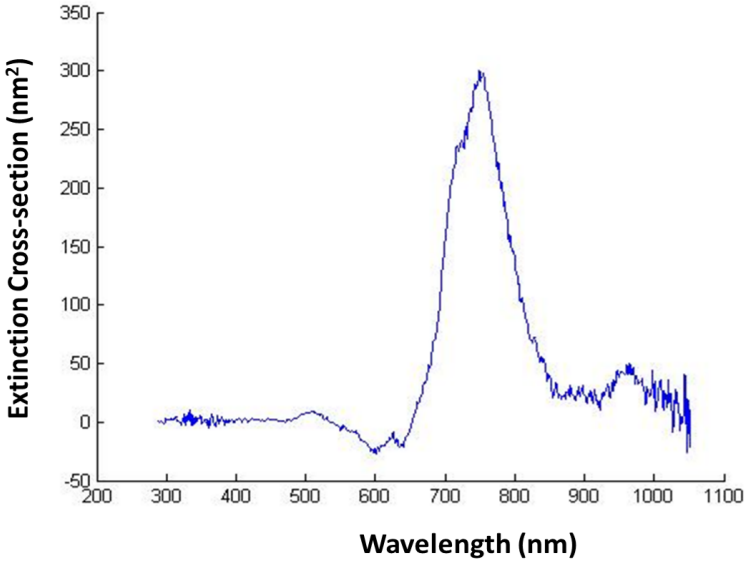


Figure 5.3: Extinction spectrum of original gold nanorod solution.

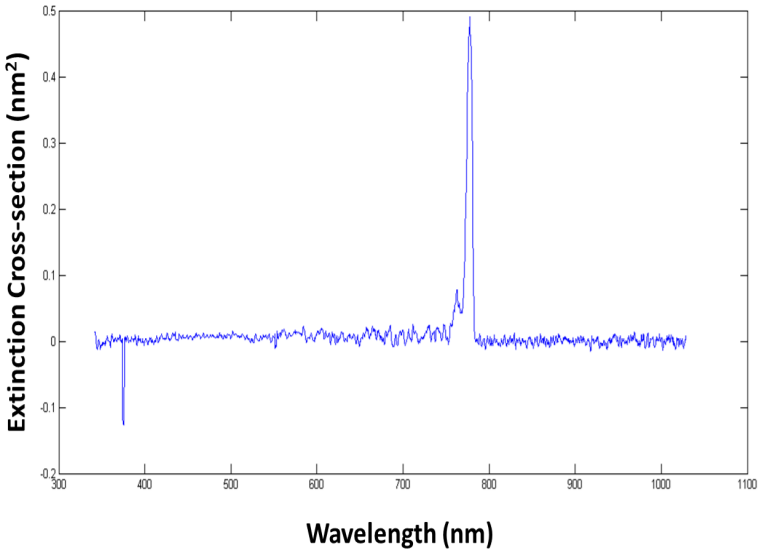


Figure 5.4: Spectrum collected for a single gold nanorod trapped.

things that resulted in this deviation from the expected (from simulation) 710 nm peak. One thing could be due to the transmission characteristics of the dichroics (at the trapping beam wavelength) placed in the spectroscopy path i.e., a leakage may resulted from the razor edge short pass filter used as a 785 nm beam block (Semrock, SP01-785RS-25). Since the beam used in the experiment has $1/e^2$ width of about 14 nm ranging from 777nm to 790nm and the notch filter has about 5% transmission at 778 (which eventually decreases to 0% transmission at 785), we observe a peak at 778 nm at the spectrometer instead of a peak at 785nm (trapping laser wavelength).

The other cause of not seeing a peak at 710 nm could be the sensitivity of the spectrometer used. Since the Ocean optics spectrometer has about 30 photons/count at 700 nm,which eventually decreases at larger wavelength than 700nm; it may not be strong enough to pick up any scattered light coming from the nanorod. Thus, it can be concluded that we may not be measuring the extinction spectrum from the trapped gold nanorod. A better result can be expected if a more sensitive spectrometer is used, preferably a spectrometer equipped with EMCCD. In which case we can assume to observe two different peaks, one at 710 nm resulting from the scattering by the trapped gold nanorod and the other at 778nm arising from the leakage through the optical train of the experimental setup.

# Chapter 6

# A Scale-based Comparative Study on Optical Tweezing: micro vs. nano

## 6.1 Introduction

Optical tweezing of micron sized objects is a straightforward technique of optical manipulation, where a 10-200 mW laser is required along with a high-NA objective to produce a potential well powerful enough to trap objects which are 1 to 20 micron in diameter [39]. Usually for micro tweezing, objects of interest are polystyrene spheres having an index of refraction larger than that of its surrounding [40]. However, optical tweezing of latex beads smaller than 300 nm diameter is difficult [25] and the forces exerted on latex particles of similar size are significantly smaller than those on corresponding

gold particles [41].

Svoboda and Block [25] first reported that the trapping forces on gold nanoparticles in the Rayleigh regime are significantly larger than on latex beads of similar size, provided that the same laser and tweezing hardware were used. Hoefelmeyer [41] also reported that forces ranging from 2.2 pN to 30 pN were exerted on gold nanoparticles whose diameter ranged from 18 to 254 nm. In both cases, laser power from 1W to 10W were required to create successful tweezing. Although it is clear that tweezing nanoparticles (made of metal or latex) requires high-power lasers of minimum 1W, this power requirement is substantially reduced when taking advantage of plasmon resonance enhancement of metal nanoparticles (particularly those consisting of Au and Ag) [21].

For this study a 130 mW semiconductor diode laser was used, which satisfied the power requirement for tweezing both the polystyrene microsphere (diameter 1.5 micron) and the Au nanorod (diameter=10nm and length=30nm, plasmon resonance enhancement is utilized). Since two different sized particles were tweezed using the same laser and hardware, a comparative study is presented below which shows the side-by-side comparison between them in terms of hardware requirement as well as differentiating them using available detection mechanisms.

## 6.2 Minimum Laser Power Requirement

From our experiment, it was evident that power requirement for the laser was much more substantial for the Au nanorod tweezing rather than the microsphere tweezing. As we took advantage of plasmon resonance enhancement (for tweezing a gold nanorod) by suitably selecting a trapping wavelength (785nm), which is slightly red-detuned from the resonance peak (760nm) of the gold nanorod used; about 60-65 mW of laser power was required to stably tweeze a single Au nanorod. On the other hand, even though maximum power available for tweezing the microsphere was 65 mW, power level close to 15 mW was seen successful enough to tweeze a single polystyrene microsphere. For the latter case, a polarizer (LPVIS100-MP, Thorlabs) was used in the beam path to reduce the laser power. For both cases, power were measured right after the spatial filter.

## 6.3 Comparison of Stiffness of Optical Tweezers

### 6.3.1 Theory

For the tweezing beam having gaussian intensity profile, the potential experienced by a particle near the focus is approximately harmonic in 3D. In one dimension (1D), the force is given by Hooks law,$F_x = -k(x - x_0)$. $k_x$ is the spring constant/stiffness/strength of the trapping potential, $x$ is the position of the particle, and $x_0$ is the equilibrium position of the particle [20]. The trapped nanorod is subject to Brownian motion as well as stochastic forces, altogether resulting in Langevin equation of motion,

$m\ddot{x} = -k_x x - \gamma\dot{x} + F(t, T)$, where $\gamma$ is the friction coefficient and $F(t, T)$ is a time and temperature dependent white noise term stemming from random collisions of the object with surrounding molecules. By Fourier transformation of the Langevin equation, a Lorentzian power spectrum is obtained [20] from which, for example, $k$ can be determined. Since the trap is nearly symmetric in the directions perpendicular to the propagation of the laser light, hence $k_x \simeq k_y$ or just evaluation of one stiffness suffices the other.

For a quantitative analysis of the trapping strength, one measure is to interpret the power spectrum of the Brownian motion of the nanorod held with the trap. In order to do so, first the time series of a gold nanoparticle performing Brownian motion in the optical trap was recorded with a photodiode and then Fourier transformed. The temporal behavior of the variance of the voltage signal was found by calculating the variance in a running time window consisting of 65,536 consecutive data points. The power spectrum analysis were performed using a Matlab software package specifically programmed for precise calibration of optical tweezers[42].

The experimental power spectrum is a stochastic function, like the nanorods position, and is fitted with its theoretical expectation value [43]; which is a Lorentzian resulting from Einstein-Ornstein-Uhlenbeck theory for Brownian motion and also takes into account the anti-aliasing filters built into the data acquisition electronics, possible 'virtual filtering' caused by the detection system, and possible aliasing caused by the finite sampling rate. Upon fitting one parameter thus determined is the corner frequency $f_c$ [44]. It describes the ratio between Stokes' friction coefficient $\gamma_0$ for rectilinear mo-

tion with constant velocity of the nanorod in water, and the trap's spring constant/trapping stiffness/strength $k$, $f_c$=$k/(2\pi\gamma_0)$. With $f_c$ and $\gamma_0$ known, the latter from Stokes' law i.e. $\gamma_0 = 6\pi\rho vR$, so is $k$ in physical units [44]. [For Stokes' Law, $\rho$ is the dynamic viscosity, $v$ is the particle's settling velocity and $R$ is the radius of the object]

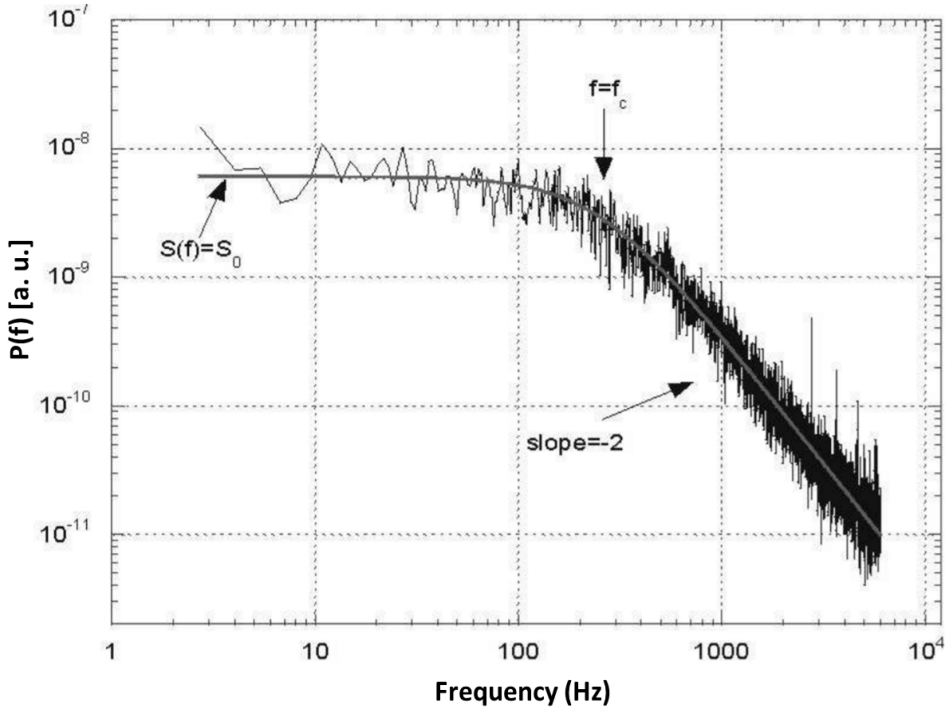


Figure 6.1: Sample power spectrum data showing corner frequency $f_c$ [27].

### Recording of time series of trapped gold nanorod

For this experiment, an interferometric technique was used for position determination and for each coordinate one time series was determined. Since a quadrant photo-diode was used as a photo detector, it measures the position (x,y) orthogonal to the beam axis as combinations of voltages from the four quadrants. If these are numbered I, II, III, and IV like the quadrants of a 2D coordinate system, and their output voltages are denoted $V_I, V_{II}, V_{III}$, and $V_{IV}$, then changes in the voltage and ratios [44]

$$R_x \equiv (V_I - V_{II} - V_{III} + V_{IV})/V_z \equiv V_x/V_z \tag{6.1}$$

$$R_x \equiv (V_I - V_{II} - V_{III} + V_{IV})/V_z \equiv V_x/V_z \tag{6.2}$$

$$V_z \equiv V_I - V_{II} - V_{III} + V_{IV} \tag{6.3}$$

are proportional to changes in the nanorod's position (x,y,z), z being the coordinate along the beam's axis. To a slightly worst approximation, x and y are proportional to $V_x$ and $V_y$. Here, the trap is calibrated only in the (x,y)-plane and only (x,y) coordinates are considered.

### Obtaining experimental power spectrum from recorded time series

The time series of positions are then Fourier transformed as a single, long series. For a coordinate x recorded at intervals $\Delta t$ for a time $T_{meas}$, the

Fourier transform is defined as [44]

$$\hat{x_n} = \Delta t \sum_{j=1}^{N} e^{i2\pi f_n t_j} x_j, \; f_n \equiv \frac{n}{T_{meas}} = n f_{sample}, \; n = 1, 2, ...., N \qquad (6.4)$$

here, $x_j$ is the value recorded for x at time $t_j = j\Delta t$, and N is the number of values recorded, $N\Delta t = T_{meas}$. The experimental power spectrum for x is then $P_x^{(ex)}(f_n) \equiv |\hat{x_n}|^2 / T_{meas}$ [44].

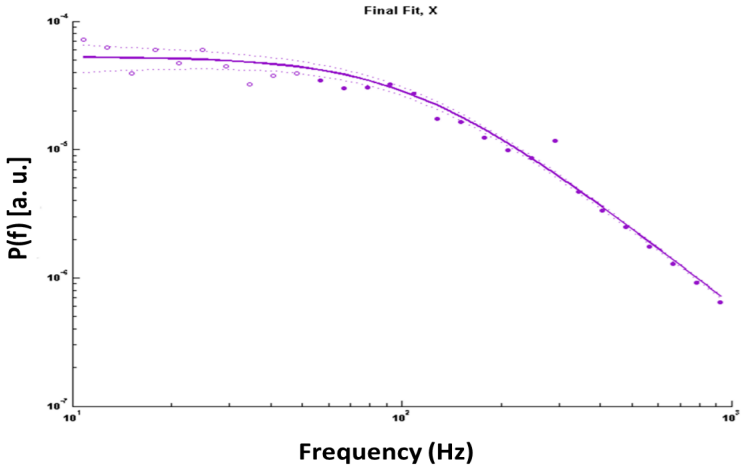


Figure 6.2: Power spectral density for a trapped gold nanorod in the x direction.

### Fitting a Lorentzian to the Experimental Power Spectrum

The theoretical spectrum fitted to the data/experimental power spectrum is a Lorentzian [44], given by

$$P^{Lorentz}(f) = \frac{D/(2\pi^2)}{f_c^2 + f^2} \qquad (6.5)$$

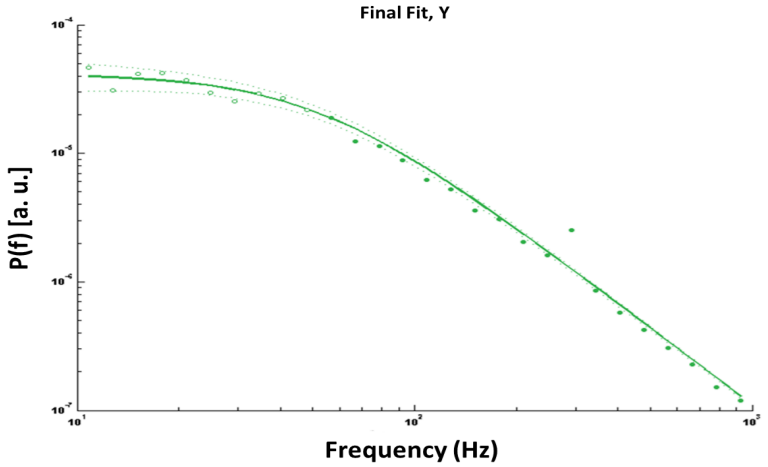


Figure 6.3: Power spectral density for a trapped gold nanorod in the y direction.

The program [42] fits the theoretical power spectrum to the experimental data using general non-linear least-squares fitting routines available with the Optimization Toolbox of MatLab (MathWorks Inc.). Blocked data points are used in order to achieve better fitting. In order to judge the quality of a given fit, the resulting value of [44]

$$\frac{\chi^2}{p_{free}} = \frac{1}{p_{free}} \sum_{n=1}^{p} \left( \frac{y_n - y_{theory}(x_n; parameters)}{\sigma_{theory}(x_n; parameters)} \right)^2 \tag{6.6}$$

is quoted along with the fitted parameter values. In the above equation p is the number of data points $(x_n, y_n)$ to which we fit, $p_{free}$ is the number of degrees of freedom, i.e., $p_{free} = p - p_{par}$ with $p_{par}$ the number of parameters added. $y_{theory}$ is the function fitted, which is the expectation value of the distribution of the data points according to the theory. The quantity $\sigma_{theory}$ is the standard deviation of this distribution. For the power spectra, $y_n =$

$P_n^{(ex)}$, $y_{theory}(x_n; parameters) = P^{theory}(f_n)$ [44].

Figure 6.2 and 6.3 are the experimental power spectra in the x axis and y axis (violet and green,respectively) and their fits (solid lines) for trapped gold nanorods with length 30 nanometers and diameter 10 nanometers at a laser power of 65 mW at the entry of the trapping objective.

### 6.3.2 Experimental setup

The experimental setup used for this experiment is the same described in the third chapter.

### 6.3.3 Results and Discussion

The measurements reported here were performed at the maximum available laser power providing stable optical trapping, this being in the range of 60-65 mW, measured at the input of the objective. The particles were trapped simply by letting them diffuse into the optical trap, which was positioned 2-6 micrometers above the surface of the cover slip, thus avoiding proximity effects [44] from the cover slip. If the suspension was not sufficiently dilute, more beads could diffuse into the trap during a measurement. In that case the trap becomes unstable.

Because our particles are small compared to the diameter of the laser focus, which is about 400 nm, they are polarized along their long axis and oriented with the electric field of the trapping laser [20]. Due to the plasmon resonances, the long axis polarizability is much higher than the one for the short axis; so that an orientation along this axis is energetically more favorable.

Thus, the particles were assumed to be aligned with the direction of polarization in our setup. The gold nanorods have the shape of a cylinder that is capped with two half-spheres, also called a spherocylinder. To calculate the values of the drag coefficient $\gamma$, in the direction of the long axis, we used the drag coeffcients for cylindrical particles, which is a good approximation for spherocylinders [45]

A gold spherocylinder fluctuating in a harmonic potential has a Gaussian distribution $P$ of positions $x$ [45], given by

$$P(x) = P_0\, e^{[(-(x-x_0)^2/2\sigma^2)]} \tag{6.7}$$

where $x_0$ is the position of the center of the trap, $P_0$ is the expected number of times the particle will be observed at $x_0$. If the above-mentioned linear relationship between position and quadrant photodiode signal holds, the measured positions should have a Gaussian distribution. Since, the theory for the trapped bead assumes a harmonic trapping potential and thereby positions visited by the trapped nanorod will rerepresent a Gaussian Boltzmann distribution. This is evident from the following figures for y position of two different traps containing one and ten nanorods.

To load the optical trap with one gold nanorod, we waited until a particle diffused into the laser focus. It typically took 1-2 hrs before a particle entered the trap. The particle(s) performed Brownian motion in the harmonic potential exerted by the optical trap. The distributions of particle positions are Gaussian, and their standard deviation increases stepwise with

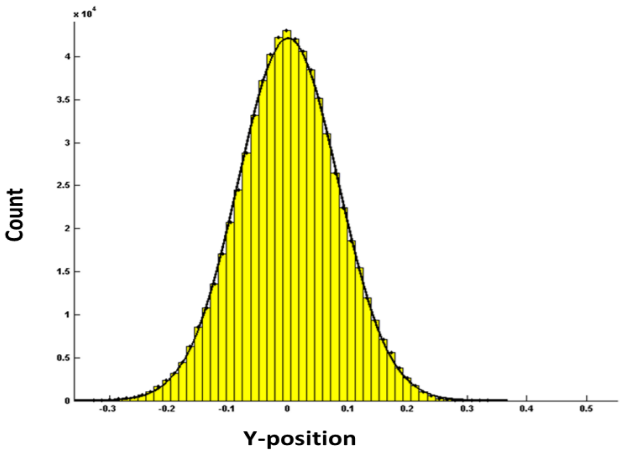


Figure 6.4: Y Position histogram and its Gaussian fit for single gold nanorod trapped, $\sigma = 0.084$.

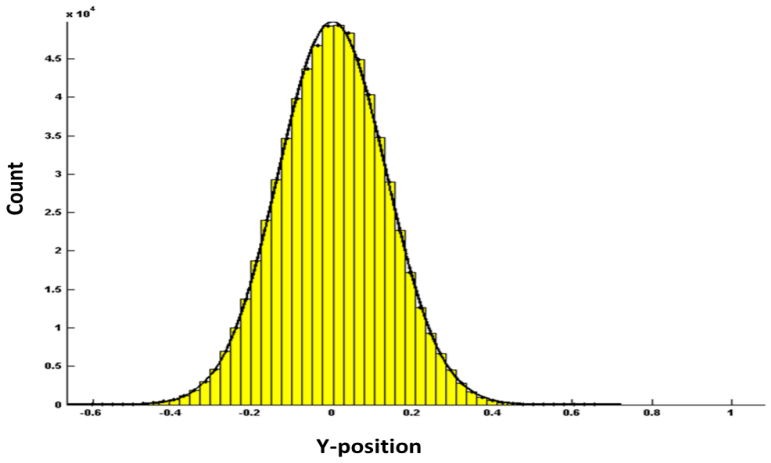


Figure 6.5: Y Position histogram and its Gaussian fit for about 10 gold nanorods trapped, $\sigma = 0.135$.

the number of particles in the trap[16, 46]. Figure 6.4 and 6.5 show position distributions from two different time intervals from the same experiment. As additional rods entered the trap, the histogram broadened. Hence, the standard deviation of a particular time series is a measure of how many particles are in the trap. The power spectral analysis was also used in order to

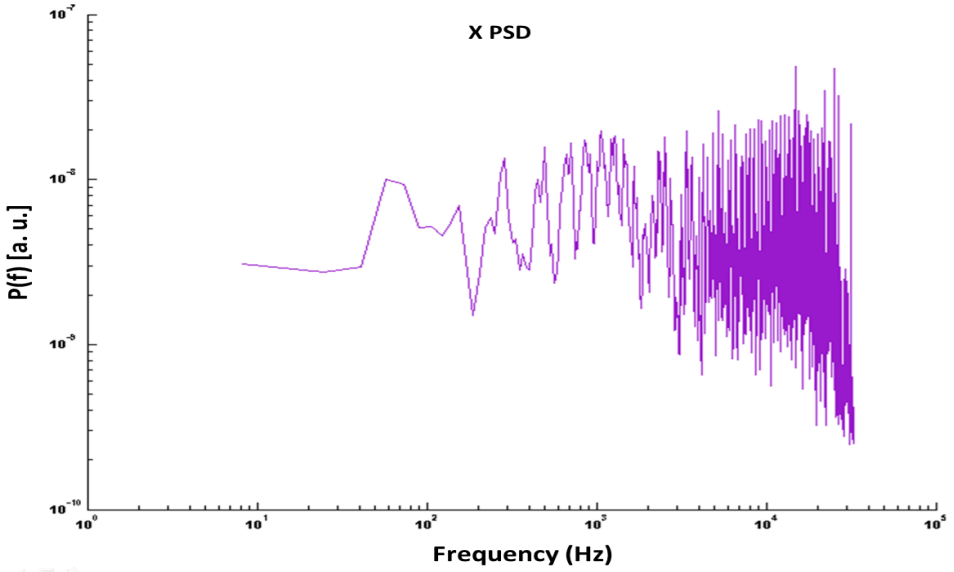


Figure 6.6: Power spectral density with no gold nanorod in the trap.

detect if any particles were trapped. As is clear from Figure 6.6, the signal from an empty trap is significantly different from that of a rod in the trap. Figure 6.7 shows power spectra of the experimentally obtained time series of the trapped single gold nanorod.

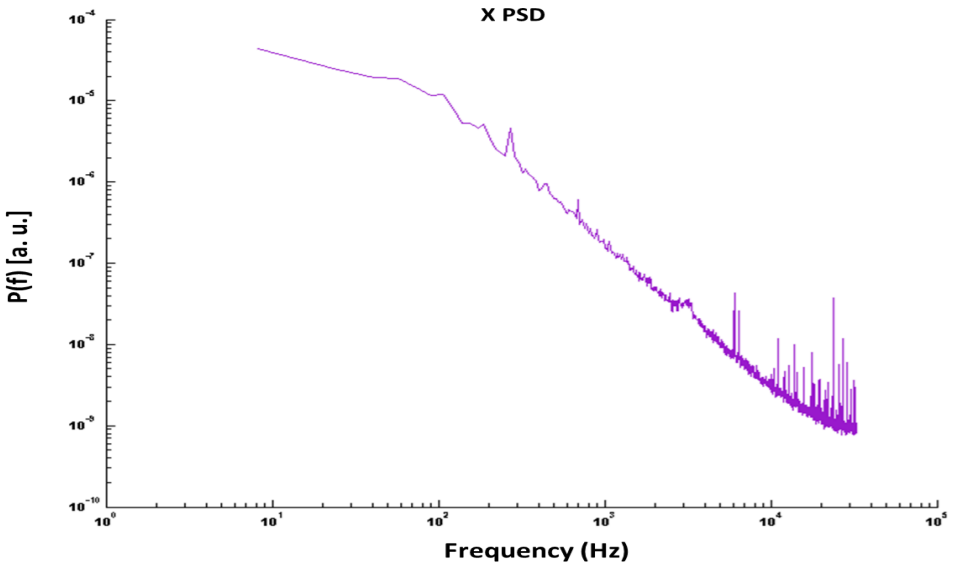


Figure 6.7: Power spectral density with single gold nanorod in the trap.

**Comparison between the trapping stiffness values of a trapped microparticle and nanoparticle**

From the table 6.1 we can see a significant difference between the trapping stiffness/spring constant values for a trapped micro- and nanoparticle. From the values it is clear that the trapping strength is directly proportional to the volume of the particle trapped. One other thing can be attributed to the lower stiffness values for the nanoparticle is the available laser power of 65 mW, which if increased could have resulted in a more powerful trap for the nanoparticle. However these values can be used if one is unsure about the nature of the trapped particle i.e., to differentiate between a trapped microparticle and a trapped nanoparticle if the stiffness values are known.

While nanoparticles are trapped, heating of the trapped object could be-

| Comparison | Micro particle | | Nano particle | |
|---|---|---|---|---|
| Dimension | radius=1.5μm | | length=30nm, radius=10nm | |
| Drag coefficient, γ (g/s) | $1.29X10^{-5}$ | | $4.435X10^{-7}$ | |
| | x axis | y axis | x axis | y axis |
| Corner frequency, $f_c$ (Hz) | 129.6 | 131.2 | 108.7 | 51.5 |
| Trap stiffness, $\kappa$ (pN/nm) | .0105 | .0106 | $3.03X10^{-4}$ | $1.43X10^{-4}$ |

Table 6.1: Comparison between trapped micro- and nanoparticle.

come an issue [8]. Heating can decrease trapping stability or lead to bubble formation. Yet, heating of gold nanoparticles in optical traps has not been directly experimentally measured and reported. In our experiments, bubble formation or other signs of heating were never observed; hence the temperature in the water surrounding the gold nanoparticle is not as high as that predicted in ref.[8]. This is probably due to two reasons: first, by compensating the spherical aberrations [47] we created an extremely efficient optical trap and used comparatively low laser powers. Second, the trapping wavelength was tuned to the long-wavelength side of the plasmon resonances, where the absorption cross section of the gold nanoparticles is significantly smaller than that at the resonance wavelength [48].

## 6.4 Comparison of Backscattered Light

### 6.4.1 Theory

While trapped by the tweezing beam, the trapped nanoparticle scatters the laser beam both in the forward and in the backward direction. When this backscattered light is collected and analysed a unique pattern for the particle trapped is observed. If the collected intensity pattern at the CCD is integrated, an unique value for that particular pattern is obtained. Hence, these patterns can be used in order to distinguish the particles being trapped. Here the backscattered patterns from the trapped nanorod are collected at the CCD and a MATLAB code is used to integrate the collected intensity pattern and thus derive a unique value from the code. Here along with integrating the CCD intensity patterns canny edge detection algoritm was also used as a tool for distinguishing the back scattered pattern.

### 6.4.2 Results and Discussion

The main distinguished feature between the two backscattered patterns created by a trapped microparticle and a nanoparticle is the diffraction pattern. The diffraction pattern created by a nanoparticle is brighter and more pronounced. As for the microparticle the diffraction pattern created is less bright and less structured.

Using Canny edge detection algoritm on both images our previous assumptions can be justified. The edges of the intensity pattern are circled in red in order to further differentiate the scattered patterns from the background.

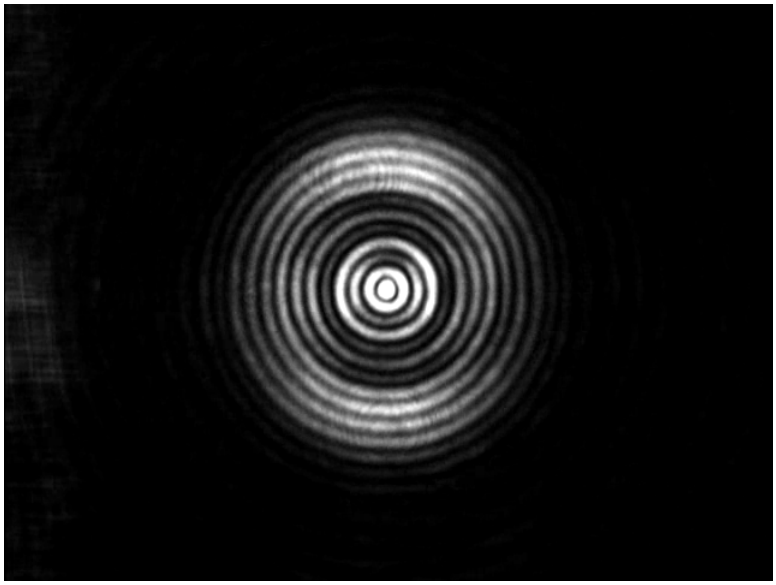

Figure 6.8: Backscattered pattern from a trapped nanoparticle.

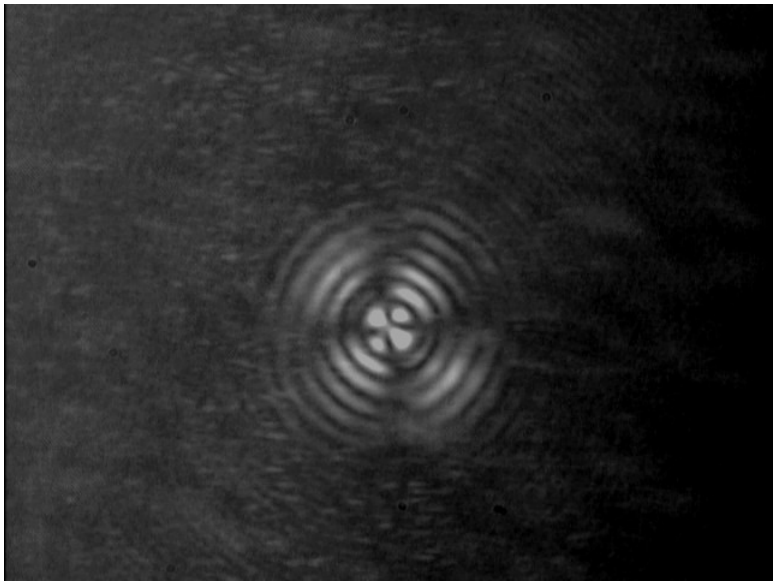

Figure 6.9: Backscattered pattern from a trapped microparticle.

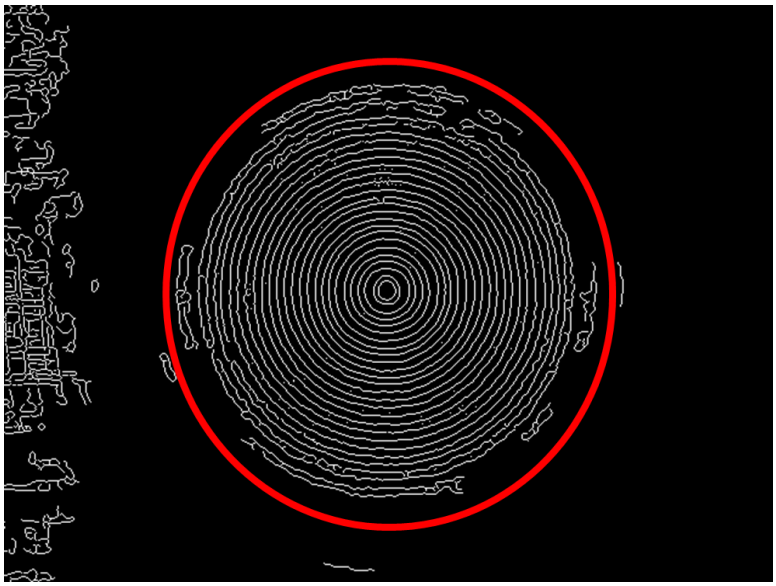

Figure 6.10: Using canny edge detection on the backscattered pattern from a trapped nanoparticle.

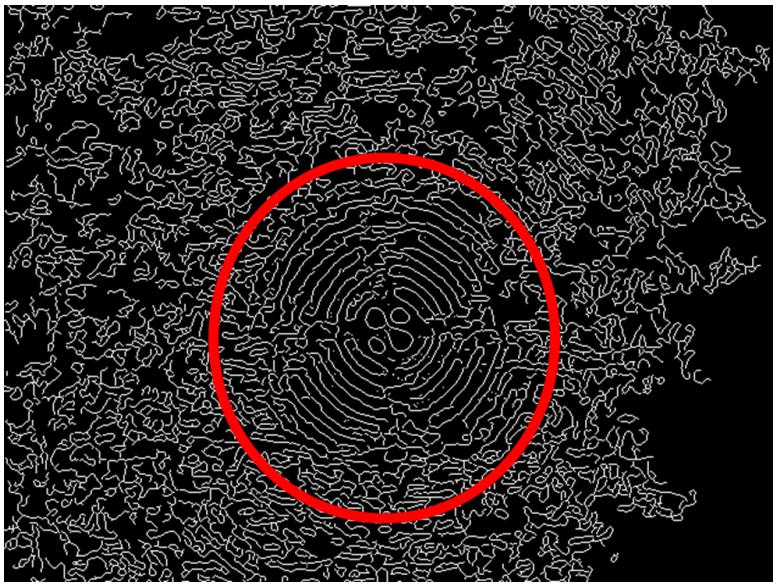

Figure 6.11: Using canny edge detection on the backscattered pattern from a trapped microparticle. For this image, the background intensity(noise) is more pronounced due to some anomalous settings of the CCD.

Again, separating only the areas of circular patterns (red circled areas) from both the images and integrating the circular intensity-pattern areas, unique values are obtained which can be easily categorized into different ranges. For the backscattered pattern created by the trapped nanorod the intensity integration usually results in much larger values compared to the backscattered patterns created by the trapped microspheres. This is further clarified in the following figure (Figure 6.12), where for each trapped particle three unique intensity values were obtained and used to create an approximate range.

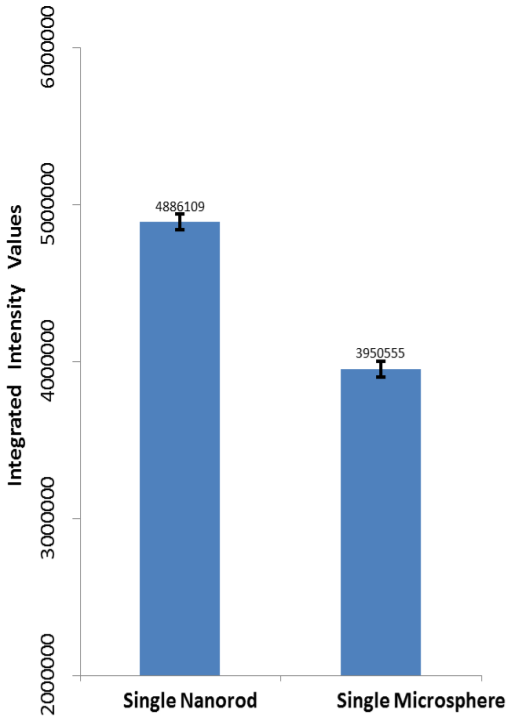


Figure 6.12: Difference in integrated intensity values obtained from the backscattered patterns.

# Chapter 7

# Conclusion

The main objective of this experiment was to develop an experimental method to optically tweeze a specific species (aspect ratio) of Au nanorod using a continuous wave laser and suggest characterization mechanisms to differentiate the single Au nanorod tweezing from standard tweezing of single polystyrene microsphere. The wavelength of the laser was predetermined from the simulated absorption and scattering spectrums for that particular species (aspect ratio) of Au nanorod. Given the maximum available power of only 65 mW, successful tweezing of gold nanorod(s) having length of 30nm and diameter of 10nm was observed. This power requirement actually depends on the trapping wavelength, which in turn depends on the location of the absortion and scattering peaks. Choosing a trapping wavelength that is further redshifted, will result in a trap with higher gradient force, which consequently reduces the power requirement of the laser to trap a single gold nanorod. In addition, an obsolete Olympus microscope (IMT-2) was reconfigured in order to use it as a platform for previously mentioned gold

nanorod trapping. Full equipment setup and procedure are provided in order to provide a thorough guideline for a beginner to adopt the plasmon resonance enhanced optical trapping technique and successfully implement it.

Characterization of the trapped nanorod was explained with the help of trapping strength, backscattered laser light and extinction spectrum. For measurement of the trapping strength, stiffness of the harmonic optical trap was used as a metric to characterize the trapped Au nanorod and later differentiate the nanorod from a dielectric microsphere. Since this trapping stiffness depends on the wavelength of the trapping laser, hence it will also depend on the species of nanoparticle used. As a result, different species of nanoparticle will give off different stiffness values for a same trapping laser (wavelength and power unchanged), provided that the trapping wavelength is redshifted from the scattering peak for all the species of nanoparticles used in the experiment. This concept can be used in future experiments where more than one species of nanoparticle that fulfills the previously mentioned criteria for stable trapping is available.

Another metric that was explored in order to differentiate Au nanorod tweezing from microsphere tweezing was the analysis of the backscattered pattern. This aspect of the experiment was basically limited by the sensitivity of the CCD camera used. Hence, a better analysis of the pattern will require a peltier cooled camera incorporated in place of the Watec CCD. Further study will constitute analysis on the change of this pattern as more nanorods get trapped and eventually compare this change of pattern to stiffness val-

ues for multiple nanorods getting trapped. Which will also result in a more robust optical trapping platform with higher precision.

Additionally, a spectroscopic charcterization of trapped gold nanorod was explored. Sensitivity of spectrometer is a large issue for this kind of experiments, for this reason a spectrometer equipped with EMCCD is usually preferred. Besides, a higher accuracy in spectral selection of the scattered light may increase the possibility of enhanced collection of scattered white light from the Au nanorod. Future applications should consist of observation of change of the extinction spectrum as single to double to multiple nanorods gets trapped. Another interesting application could be the effect of rotation of the nanorod on the intensity of the extinction spectrum peak. This increase in intensity may result from the colinearity of the long axis of the nanorod with incident white light polarization [22].At the same time, forward scattered light from the trapped nanoparticle can be collected at the photo-detector to gain trapping strength values, which later could be incorporated in order to provide a better understanding of single to multiple particle trapping on trapping stiffness.

# Chapter 8

# Appendix

(1)Tweezercalib 2.0: This MatLab package was used with MathWorks MatLab 2010a on a personal computer running Windows 7 Professional (x64).

This package was used to precisely calibrate the optical tweezers presented in this thesis. The calibration is based on the power spectrum of the Brownian motion of a dielectric bead trapped in the tweezers. Precision is achieved by accounting for a number of factors that affect this power spectrum i.e. elimination of cross-talk between quadrant photo-diodes output channels for positions, data compression and noise reduction by blocking method, accounting for electronic filters and accounting for aliasing caused by finite sampling rate [42].

Input data for this package should be positions of bead doing Brownian motion while trapped by the optical tweezers. For high precision in final results, data should be time series measured over a long time (30 seconds), with sufficiently high sampling rate. The sampling rate should be well above

the characteristic frequency of the trap (corner frequency). Thus, the sampling frequency should typically be larger than 10 kHz. The Fast Fourier Transform works optimally when the time series contain $2^n$ data points with n=(12-15) [42].

Package obtainable from: CPC Program Library, Queens University of Belfast, N. Ireland.

(2)Timescan.vi: The following LabView code was written and conducted in LabView 2009 running on Windows 7 operating system.

This LabView code was used in order to convert voltage signals collected from the photodetector into timeseries data, which represented position of the trapped particle relative to the centre of the trap over the duration of collection period (10 seconds).

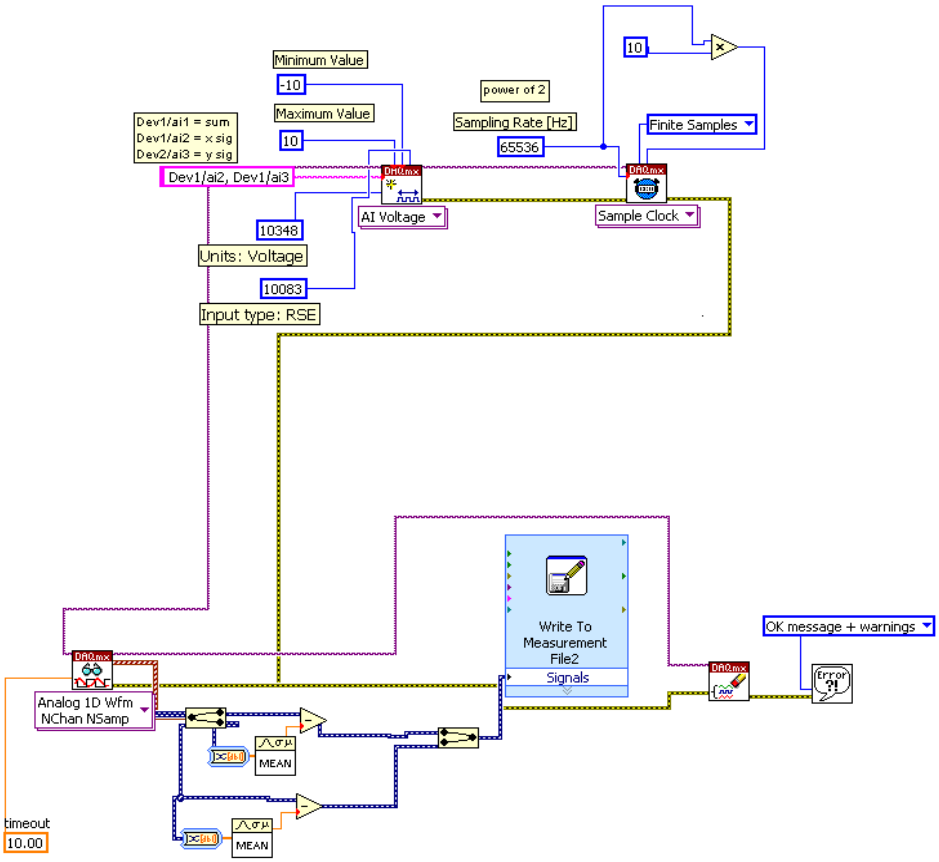


Figure A.1: Block diagram of timescan.vi

# References


[1] A. Ashkin. Optical trapping and manipulation of neutral particles using lasers. *Proceedings of the National Academy of Sciences of the United States of America*, 94(10):4853–4860, 1997.

[2] Woei Ming Lee, Peter J Reece, Robert F Marchington, Nikolaus K Metzger, and Kishan Dholakia. Construction and calibration of an optical trap on a fluorescence optical microscope. *Nature Protocols*, 2(12):3226–3238, 2007.

[3] A. Ashkin, J.M. Dziedzic, J.E. Bjorkholm, and S. Chu. Observation of a single-beam gradient force optical trap for dielectric particles. *Optics Letters*, 11(5):288–290, 1986.

[4] K. Dholakia and P. Reece. Optical micromanipulation takes hold. *Nano Today*, 1(1):18–27, 2006.

[5] J. Plewa, E. Tanner, D.M. Mueth, and D.G. Grier. Processing carbon nanotubes with holographic optical tweezers. *Optics Express*, 12(9):1978–1981, 2004.

[6] Karel Svoboda and Steven M. Block. Optical trapping of metallic rayleigh particles. *Optics Letters*, 19(13):930–932, 1994.

[7] J. Prikulis, F. Svedberg, M. Kll, J. Enger, K. Ramser, M. Goksr, and D. Hanstorp. Optical spectroscopy of single trapped metal nanoparticles in solution. *Nano Letters*, 4(1):115–118, 2004.

[8] Y. Seol, A.E. Carpenter, and T.T. Perkins. Gold nanoparticles: Enhanced optical trapping and sensitivity coupled with significant heating. *Optics Letters*, 31(16):2429–2431, 2006.

[9] A. Ashkin and J.M. Dziedzic. Observation of resonances in the radiation pressure on dielectric spheres. *Physical Review Letters*, 38(23):1351–1354, 1977.

[10] S. Chu, J.E. Bjorkholm, A. Ashkin, and A. Cable. Experimental observation of optically trapped atoms. *Physical Review Letters*, 57(3):314–317, 1986.

[11] R.R. Agayan, F. Gittes, R. Kopelman, and C.F. Schmidt. Optical trapping near resonance absorption. *Applied Optics*, 41(12):2318–2327, 2002.

[12] D.T. Chiu and R.N. Zare. Biased diffusion, optical trapping, and manipulation of single molecules in solution. *Journal of the American Chemical Society*, 118(27):6512–6513, 1996.

[13] T. Iida and H. Ishihara. Theoretical study of the optical manipulation of semiconductor nanoparticles under an excitonic resonance condition. *Physical Review Letters*, 90(5):057403/1–057403/4, 2003.

[14] M. Pelton, T. Iida, and H. Ishihara. Comment on "theoretical study of the optical manipulation of semiconductor nanoparticles under an excitonic resonance condition" [2] (multiple letters). *Physical Review Letters*, 92(8):897011–897021, 2004.

[15] M. Pelton, M. Liu, S. Park, N.F. Scherer, and P. Guyot-Sionnest. Ultrafast resonant optical scattering from single gold nanorods: Large nonlinearities and plasmon saturation. *Physical Review B - Condensed Matter and Materials Physics*, 73(15), 2006.

[16] P.M. Hansen, V.K. Bhatia, N. Harrit, and L. Oddershede. Expanding the optical trapping range of gold nanoparticles. *Nano Letters*, 5(10):1937–1942, 2005.

[17] Lana Bosanac, Thomas Aabo, Poul M Bendix, and Lene B Oddershede. Efficient optical trapping and visualization of silver nanoparticles. *Nano Letters*, 8(5):1486–1491, 2008.

[18] Y. Zhang, C. Gu, A.M. Schwartzberg, S. Chen, and J.Z. Zhang. Optical trapping and light-induced agglomeration of gold nanoparticle aggregates. *Physical Review B - Condensed Matter and Materials Physics*, 73(16), 2006.

[19] P H Jones, F Palmisano, F Bonaccorso, P G Gucciardi, G Calogero, A C Ferrari, and O M Marag. Rotation detection in light-driven nanorotors. *ACS nano*, 3(10):3077–3084, 2009.

[20] Christine Selhuber-Unkel, Inga Zins, Olaf Schubert, Carsten Snnichsen, and Lene B Oddershede. Quantitative optical trapping of single gold nanorods. *Nano Letters*, 8(9):2998–3003, 2008.

[21] K.C. Toussaint Jr., M. Liu, M. Pelton, J. Pesic, M.J. Guffey, P. Guyot-Sionnest, and N.F. Scherer. Plasmon resonance-based optical trapping of single and multiple au nanoparticles. *Optics Express*, 15(19):12017–12029, 2007.

[22] Lianming Tong, Vladimir D Miljkovi, and Mikael Kll. Alignment, rotation, and spinning of single plasmonic nanoparticles and nanowires using polarization dependent optical forces. *Nano Letters*, 10(1):268–273, 2010.

[23] C.F. Bohren and D.R. Huffman. *Absorption and Scattering of Light by Small Particles*. John Wiley & Sons, New York, 1983.

[24] M.J. Lang, P.M. Fordyce, A.M. Engh, K.C. Neuman, and S.M. Block. Simultaneous, coincident optical trapping and single-molecule fluorescence. *Nat Methods*, 1(2):133–139, 2004.

[25] K. Svoboda and S.M. Block. Biological applications of optical forces. *Annual Review of Biophysics and Biomolecular Structure*, 23:247–285, 1994.

[26] A. Ashkin. Forces of a single-beam gradient laser trap on a dielectric sphere in the ray optics regime. *Methods in Cell Biology*, (55):1–27, 1998.

[27] Demetrious Mark Harrington. Construction and calibration of a laser tweezers apparatus using a fast camera. *Senior Thesis*, 2005.

[28] Brooke C. Hester, Rani B. Kishore, Kristian Helmerson, Naomi J. Halas, and Carly Levin. Optical trapping of nanoshells near resonance. *Plasmonics: Metallic Nanostructures and Their Optical Properties VI*, 7032(1):70321Z, 2008.

[29] A. Yariv. *Quantum Electronics*. John Wiley and Sons, Inc., 1967.

[30] Michael Faraday. The bakerian lecture: Experimental relations of gold (and other metals) to light. *Philosophical Transactions of the Royal Society of London*, 147:pp. 145–181, 1857.

[31] Suchita A Kalele, Neha R Tiwari, Suresh W Gosavi, and Sulabha K Kulkarni. Plasmon-assisted photonics at the nanoscale. *Journal of Nanophotonics*, 1(1):012501, 2007.

[32] Gustav Mie. Beitrge zur optik trber medien, speziell kolloidaler metallsungen. *Annalen der Physik*, 330(3):377–445, 1908.

[33] K. Lance Kelly, Eduardo Coronado, Lin Lin Zhao, and George C. Schatz. The optical properties of metal nanoparticles: the influence of size, shape, and dielectric environment. *The Journal of Physical Chemistry B*, 107(3):668–677, 2003.

[34] Yugang Sun and Younan Xia. Gold and silver nanoparticles: A class of chromophores with colors tunable in the range from 400 to 750 nm. *Analyst*, 128:–, 2003.

[35] Babak Nikoobakht and Mostafa A. El-Sayed. Preparation and growth mechanism of gold nanorods (nrs) using seed-mediated growth method. *Chemistry of Materials*, 15(10):1957–1962, 2003.

[36] Kaspar D. Ko and Kimani C. Toussaint Jr. A simple gui for modeling the optical properties of single metal nanoparticles. *Journal of Quantitative Spectroscopy and Radiative Transfer*, 110(12):1037 – 1043, 2009.

[37] Jack J. Mock, David R. Smith, and Sheldon Schultz. Local refractive index dependence of plasmon resonance spectra from individual nanoparticles. *Nano Letters*, 3(4):485–491, 2003.

[38] Juris Prikulis, Fredrik Svedberg, Mikael Kll, Jonas Enger, Kerstin Ramser, Mattias Goksr, and Dag Hanstorp. Optical spectroscopy of single trapped metal nanoparticles in solution. *Nano Letters*, 4(1):115–118, 2004.

[39] Stephen P. Smith, Sameer R. Bhalotra, Anne L. Brody, Benjamin L. Brown, Edward K. Boyda, and Mara Prentiss. Inexpensive optical tweezers for undergraduate laboratories. *American Journal of Physics*, 67(1):26–35, 1999.

[40] Erik Fällman and Ove Axner. Influence of a glass-water interface on the on-axis trapping of micrometer-sized spherical objects by optical tweezers. *Appl. Opt.*, 42(19):3915–3926, Jul 2003.

[41] James D Hoefelmeyer, Krisztian Niesz, Gabor A Somorjai, and T Don Tilley. Expanding the optical trapping range of gold nanoparticles. *Nano Letters*, 5(3):1937–1942, 2005.

[42] P.M. Hansen, I.M. Tolic-Nrrelykke, H. Flyvbjerg, and K. Berg-Srensen. tweezercalib 2.1: Faster version of matlab package for precise calibration of optical tweezers. *Computer Physics Communications*, 175(8):572–573, 2006.

[43] Frederick Gittes and Christoph F. Schmidt. Chapter 8 signals and noise in micromechanical measurements. 55:129 – 156, 1997.

[44] Iva Marija Toli-Nrrelykke, Kirstine Berg-Srensen, and Henrik Flyvbjerg. Matlab program for precision calibration of optical tweezers. *Computer Physics Communications*, 159(3):225 – 240, 2004.

[45] H. Lwen. Brownian dynamics of hard spherocylinders. *Physical Review E*, 50(2):1232–1242, 1994.

[46] L. Bosanac, T. Aabo, P.M. Bendix, and L.B. Oddershede. Efficient optical trapping and visualization of silver nanoparticles. *Nano Letters*, 8(5):1486–1491, 2008.

[47] S.N.S. Reihani and L.B. Oddershede. Optimizing immersion media refractive index improves optical trapping by compensating spherical aberrations. *Optics Letters*, 32(14):1998–2000, 2007.

[48] Maria Dienerowitz, Michael Mazilu, Peter J. Reece, Thomas F. Krauss, and Kishan Dholakia. Optical vortex trap for resonant confinement of metal nanoparticles. *Opt. Express*, 16(7):4991–4999, Mar 2008.